Numerical study of the effects of gravity on soot formation in laminar coflow methane/air diffusion flames under different air stream velocities

Kong, Wenjun; Liu, Fengshan

Publisher's version / Version de l'éditeur:
https://doi.org/10.1081/13647830903342527
Combustion Theory and Modelling, 13, 6, pp. 993-1023, 2009

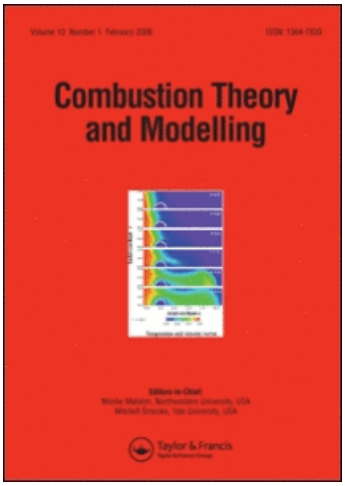

Combustion Theory and Modelling
Publication details, including instructions for authors and subscription information:
http://www.informaworld.com/smpp/title~content=t713665226

Numerical study of the effects of gravity on soot formation in laminar coflow methane/air diffusion flames under different air stream velocities

Wenjun Kong [a]; Fengshan Liu [b]
[a] Institute of Engineering Thermophysics, Chinese Academy of Sciences, Beijing, China [b] Institute for Chemical Process and Environmental Tech., National Research Council Canada, Ottawa, Canada

Online publication date: 05 February 2010

To cite this Article Kong, Wenjun and Liu, Fengshan(2009) 'Numerical study of the effects of gravity on soot formation in laminar coflow methane/air diffusion flames under different air stream velocities', Combustion Theory and Modelling, 13: 6, 993 — 1023
To link to this Article: DOI: 10.1080/13647830903342527
URL: http://dx.doi.org/10.1080/13647830903342527

Combustion Theory and Modelling
Vol. 13, No. 6, 2009, 993–1023

Numerical study of the effects of gravity on soot formation in laminar coflow methane/air diffusion flames under different air stream velocities

Wenjun Kong[a] and Fengshan Liu[b*]

[a]*Institute of Engineering Thermophysics, Chinese Academy of Sciences, Beijing, China;*
[b]*Institute for Chemical Process and Environmental Tech., National Research Council Canada, Ottawa, Canada*

(*Received 10 February 2009; final version received 2 September 2009*)

Numerical simulations of laminar coflow methane/air diffusion flames at atmospheric pressure and different gravity levels were conducted to gain a better understanding of the effects of gravity on soot formation by using relatively detailed gas-phase chemistry and complex thermal and transport properties coupled with a semi-empirical two-equation soot model. Thermal radiation was calculated using the discrete-ordinates method coupled with a non-grey model for the radiative properties of CO, CO_2, H_2O, and soot. Calculations were conducted for three coflow air velocities of 77.6, 30, and 5 cm/s to investigate how the coflowing air velocity affects the flame structure and soot formation at different levels of gravity. The coflow air velocity has a rather significant effect on the streamwise velocity and the fluid parcel residence time, especially at reduced gravity levels. The flame height and the visible flame height in general increase with decreasing the gravity level. The peak flame temperature decreases with decreasing either the coflow air stream velocity or the gravity level. The peak soot volume fraction of the flame at microgravity can either be greater or less than that of its normal gravity counterpart, depending on the coflow air velocity. At sufficiently high coflow air velocity, the peak soot volume fraction increases with decreasing the gravity level. When the coflow air velocity is low enough, soot formation is greatly suppressed at microgravity and extinguishment occurs in the upper portion of the flame with soot emission from the tip of the flame owing to incomplete oxidation. The numerical results provide further insights into the intimate coupling between flame size, residence time, thermal radiation, and soot formation at reduced gravity level. The importance of thermal radiation heat transfer and coflow air velocity to the flame structure and soot formation at microgravity is demonstrated for the first time.

Keywords: soot formation; laminar diffusion flame; microgravity combustion; thermal radiation; coflow air velocity

1. Introduction

In microgravity (0 g) the elimination of buoyancy-induced flows significantly prolongs the residence time associated with combustion, leading to the enhancement of both soot production and oxidation. At 0 g radiation becomes more important even for small diffusion flames [1]. Radiation is strongly coupled with soot and other flame processes through its

*Corresponding author. Email: Fengshan.Liu@nrc-cnrc.gc.ca

ISSN: 1364-7830 print / 1741-3559 online

DOI: 10.1080/13647830903342527
http://www.informaworld.com

strong impact on temperature. Thus a better understanding of the intimate coupling between residence time, soot formation, and radiation in 0 g laminar diffusion flames is of great importance not only fundamentally, but also practically, since it is directly relevant to fire safety aboard spacecraft [1, 2].

There have been many experimental studies on the structure and sooting behaviour of non-buoyant diffusion flames [3–16]. Earlier experimental studies focused on the transient behaviour of the flame when it is suddenly subject to 0 g from normal gravity (1 g) using drop tower [3, 5, 6] and the overall flame shape (diameter, length) and appearance [4, 7, 8]. More recent experimental investigations at 0 g examined the smoke point properties [9, 15, 16] and measured soot volume fraction distributions [11–15]. However, it is observed that in almost all of these experimental studies the jet diffusion flames were generated without the co-flowing air, i.e. the fuel burns in quiescent air [12, 13]. An exception to this observation is the study by Lin and Faeth [17], who experimentally and theoretically investigated the effect of the co-flowing air on the shape of non-buoyant laminar diffusion flames generated at reduced pressures. The results reveal the importance of the flow field on the diffusion flame structure and the ultimate soot volume fraction. More recently, Vietoris *et al.* [18] and Brahmi *et al.* [19] extended the above studies to a diffusion flame established in a non-buoyant laminar boundary layer, which is closer to a fire scenario aboard a spacecraft. They found that the luminosity of a 0 g diffusion flame increased with the oxidiser stream velocity, an observation in contrast to the previous findings that extended residence times lead to more soot production, e.g. [15]. Legros *et al.* [20] further investigated the influence of the oxidiser velocity on soot concentrations showing that increasing the oxidiser velocity enhanced both soot oxidation and soot formation. To provide further evidence on such observations, Fuentes *et al.* [21] focused on the soot trajectory in a non-buoyant, laminar, flat plate, boundary layer diffusion flame similar to that of Brahmi *et al.* [19]. Their results shown that local soot volume fractions are a function of the local formation and oxidation residence times and are not necessarily related to the global residence time.

Owing to the costs and difficulties in conduct 0 g experiments, it is very challenging to obtain all the parameters that are of interest to understand their effects on soot formation and flame structure in 0 g. These difficulties are associated with the limited numbers of experiments that can be conducted, the limited weight and space available for the experimental setup, and the limited duration of microgravity using either a space shuttle or a drop-tower. The last limitation also excludes investigations of relatively large diffusion flames, where the effects of thermal radiation and residence time on soot formation are expected to be more pronounced, owing to their relatively long relaxation to steady state after ignition. As a consequence, only a few compact measurement apparatus can be used in microgravity environment, which means only limited information can be obtained. Thus, numerical modeling is a valuable tool to gain insights into the effects of gravity on soot formation and provide information, which is otherwise inaccessible experimentally, such as the velocity and temperature fields and species concentration distributions, to help gain deeper insights into the influences of buoyancy on soot formation and the flame structure in general.

Significant research efforts have been devoted to understand the formation mechanisms of combustion-generated soot and the effects of various physical factors (gravity, pressure, co-flow air velocity, partial premixing, burner arrangement etc.) on soot in the last few decades. Although progress has been made in the chemical mechanisms for soot inception and surface growth, our understanding is far from certain and complete given the very different views on these processes, e.g. [22, 23]. Development of comprehensive and robust combustion models has been greatly impeded by our limited understanding of soot

inception and surface growth processes in hydrocarbon fuelled flames. Even so, simplified semi-empirical soot formation models have been demonstrated to be useful to gain insights into the effects of certain physical factors on the flame structure and soot formation, such as in [24] (gravity effect), [25] (burner arrangement), and [26] (pressure effect).

Although a number of studies on numerical simulations of soot formation in axisymmetric coflow diffusion flames at earth gravity and atmospheric pressure have been carried out in the last decade, e.g. [27–30], there have been only a few numerical studies on the effects of gravity on soot formation and the structure of laminar axisymmetric coflow diffusion flame. The only closely relevant two numerical studies are those of Kaplan *et al.* [24] and Walsh *et al.* [31]. Kaplan *et al.* [24] numerically investigated the effects of gravity on an axisymmetric laminar ethylene jet diffusion flame generated by issuing the fuel from a 1 cm diameter fuel tube into quiescent air, rather than into coflowing air. In the study of Kaplan *et al.* [24], the time-dependent reactive-flow Navier–Stokes equations coupled with a phenomenological chemical reaction model and a fuel based global soot model were solved to investigate the effects of gravity on the dynamics and behaviour of this ethylene diffusion flame under different gravity conditions. Their numerical results showed that soot production was greatly enhanced at 0 g with the peak soot volume fraction increased by as much as a factor of 11 over that at 1 g. Such predicted enhancement in the peak soot volume fraction is much greater than available experimental measurements conducted in a 2.2 s drop tower [10, 11]. The measurements of Megaridis *et al.* [10] in a diluted acetylene (by 50% nitrogen) jet diffusion flame in still air showed that the peak soot volume fraction in 0 g is about twice that at 1 g. The finding of a factor of 2 enhancement of the peak soot volume fraction in the 50% nitrogen diluted acetylene flame at 0 g was later confirmed by Greenberg and Ku [11]. Kaplan *et al*. [24] attributed the overprediction in the peak soot volume fraction to the differences in fuel type and flow rate between their numerical modelling and the experimental measurements and the insufficient relaxation time available in the experiments. The large differences between the computations and the experimental results suggest that more efforts are needed for simulations of soot formation in microgravity. Walsh *et al.* [31] conducted an experimental and computational study of nitrogen diluted methane/air laminar coflow diffusion flames at 1 g and 0 g. Unfortunately, they only considered conditions under which the flames are lifted and essentially no soot is formed.

In view of the above literature survey on the different influences of residence time on soot formation under different flame conditions and a lack of adequate numerical studies on the effect of gravity on soot formation in axisymmetric coflow diffusion flames at 0 g, therefore, the purpose of this study is to investigate the effect of gravity on soot formation and the flame structure under different coflow air velocities by conducting detailed numerical calculations using detailed gas-phase chemistry and complex thermal and transport properties.

2. Numerical method

The elliptic governing equations of mass, momentum, energy and species in the low Mach number limit and in axisymmetric cylindrical coordinates (r, z) described in [32, 33] are solved. The gravitational term is included in the momentum equation along z (vertically upwards) direction. The effects of buoyancy on the flame structure and soot formation characteristics under different gravity levels can be easily modelled by varying the value of the gravitational acceleration, which is 980 cm/s^2 at 1 g. The method of correction diffusion velocity described in [34] was employed to ensure that the net diffusion flux of all species sums to zero in both r and z directions. Note that the correction velocity

accounts for the thermophoretic velocity of soot. The interaction between the soot chemistry and the gas-phase chemistry was accounted for through the reaction rates of the species related to soot formation and oxidation, namely C_2H_2, CO, H_2, O_2, O, H, and OH in the present context. Only the thermal diffusion velocities of H_2 and H were taken into account using the expression given in [34]. The source term in the energy equation owing to radiation heat transfer was included and calculated using the method described below.

A modified version of the semi-empirical two-equation formulation of soot kinetics proposed by Leung *et al.* [35] was used to model soot nucleation, surface growth and oxidation. In this simplified soot nucleation and growth model, it is assumed that acetylene is the only soot nucleation and growth species and soot nucleation and surface growth proceed respectively via $C_2H_2 \rightarrow 2C(S) + H_2$ and $C_2H_2 + nC(S) \rightarrow (n+2)C(S) + H_2$. The rates of nucleation and surface growth are given as $R_1 = k_1(T)[C_2H_2]$ (kmol/m^3/s) and $R_2 = k_2(T)A_s^{0.5}[C_2H_2]$ (kmol/m^3/s), where $A_s = \pi(6/\pi)^{2/3}\rho_{C(S)}^{-2/3}Y_s^{2/3}\rho N^{1/3}$ is the soot surface area per unit volume and $[C_2H_2]$ is the mole concentration of acetylene. The nucleation and growth rate constants used in the present calculations were taken from a previous study [36]: $k_1 = 1000\exp(-16103/T)$ [1/s] and $k_2 = 1750\exp(-10064/T)$ [m$^{0.5}$/s]. The density of soot $\rho_{C(S)}$ is assumed to be 1.9 g/cm^3. It is noted that the soot surface growth rate is assumed here to be proportional to the square root of the soot surface area based on the recommendation of Leung *et al.* [35]. Soot oxidation was assumed to proceed through the following reactions: $O_2 + 0.5C(S) \rightarrow CO$, $OH + C(S) \rightarrow CO + H$, and $O + C(S) \rightarrow CO$. Further details of the governing equations and soot model can be found in [32, 33].

The radiation source term in the energy equation was calculated using the discrete-ordinates method (DOM) in axisymmetric cylindrical geometry. The corresponding T_3 quadrature given in [29] was used for the angular discretisation. Spatial discretisation of the radiative transfer equation was achieved using the finite volume method along with the central difference scheme. The efficient implementation approach of the statistical narrow-band correlated-k (SNBCK) based wide band model described by Liu and Smallwood [37] was employed to obtain the absorption coefficients of the combustion products containing CO, CO_2, H_2O, and soot at each wide band. In this model, the radiative properties of CO, CO_2, and H_2O are evaluated using the SNB parameters of Soufiani and Taine [38], while the spectral absorption coefficient of soot was obtained by Rayleigh's theory for small particles and assumed to be $5.5 f_v/\lambda$ with f_v being the soot volume fraction and λ the wavelength at the band centre.

The density of the mixture (including soot) was calculated using the ideal gas state equation. Gas-phase combustion chemistry was modeled using the GRI-Mech 3.0 mechanism [39], which was optimised for methane combustion, with the removal of species and reactions related to NO_x formation (except N_2). This simplified GRI-Mech 3.0 mechanism contains 36 species and 219 reactions. Thermal and transport properties of species and the mixture were obtained from CHEMKIN subroutines and the GRI-Mech 3.0 database. To allocate the flame front where the mixture fraction is stoichiometric, the mixture fraction field was calculated using the definition of Bilger *et al.* [40].

The fully coupled transport equations were discretised by the standard finite volume method. The SIMPLE algorithm for pressure-velocity coupling was employed. The discretised equations of momentum, pressure correction, temperature, soot mass fraction, and soot number density were solved using the tri-diagonal matrix algorithm. Equations of gas-phase species were solved simultaneously using a direct solver at each control volume. Furthers details are available in [32] and [33].

This simplified soot model, when used in conjunction with the GRI-Mech 3.0 mechanism [39], has been shown to perform quite well in the prediction of laminar coflow CH_4/air diffusion flames at atmospheric [29] and elevated pressures [26]. In addition, the effect of gravity on soot formation is believed to be a physical phenomenon, rather than a chemical one. For these reasons, it is appropriate to use this simplified soot formation model for the purposes of the present study.

3. Results and discussions

The laminar methane/air flame investigated in this study is generated using an axisymmetric coflow diffusion flame burner in which the fuel stream is delivered through the central fuel pipe of 10.9 mm internal diameter (0.9 mm thickness) while the coflowing air stream is delivered through the co-annular region between the fuel pipe and an outer pipe of 26 cm inner diameter. The fuel tube size considered in this study is identical to that of the Gülder burner [41] and very similar to that of the Santoro burner [42] (11.1 mm) and the fuel pipe diameter considered in the numerical study of Kaplan *et al.* [24] (10 mm). These burners have been used extensively to study soot formation in laminar diffusion flames at atmospheric pressure and 1 g. Uniform inlet temperatures of 300 K are assumed for both the fuel and air streams. The temperature at the burner rim is also kept at 300 K. The velocity distribution at the exit of the fuel pipe is assumed to be parabolic shaped corresponding to a fully developed round pipe flow, i.e. $2v_F[1 - (r/R_I)^2]$, where r is the radial position, R_I is the inner radius of the fuel tube, and v_F is the mean velocity of the fuel. The mean velocity is defined as the ratio of the volumetric flow rate of the fuel and the cross-sectional area of the fuel pipe. The mean fuel stream velocity is fixed at $v_F = 6.5$ cm/s throughout this study. The inlet velocity at the air stream remains uniform at the specified velocity outside the boundary layer formed on the outer surface of the fuel pipe. A boundary layer type velocity distribution close to the fuel pipe is assumed. The fuel flow rate was chosen to produce a visible flame height of about 64 mm at the highest coflow air velocity considered (77.6 cm/s) and 1 g. Conditions corresponding to this visible flame height have been used previously in several experimental and numerical studies of a laminar ethylene diffusion flame at 1 g [36, 41]. To investigate the effect of the coflow air velocity, three coflow air velocities of $v_A = 77.6$, 30, and 5 cm/s were considered in the calculations. Non-uniform grids were used in both$r$ and$z$directions to provide greater resolution in the large gradient regions without an excessive increase in the computing time. Fine grids were placed in the r direction between 0 and 1 cm with a grid resolution of about 0.16 mm. In the streamwise direction, fine grids were used in the burner exit region and the grid gradually became coarser as the distance from the burner exit increased. The dimensions of the solution domain were 9.78 cm in the streamwise direction and 13 cm in the radial direction. In total, the computational domain was divided into 251 (z) $\times$ 135 (r) control volumes. Inlet conditions were specified for the fuel and air streams at the $z = 0$ boundary. Symmetry conditions were used at the centreline, i.e. $r = 0$. Free slip conditions were assumed for the velocity at the outer $r = 13$ cm boundary. Zero-gradient conditions were enforced at the top exit boundary. In the calculation of radiation heat transfer, all the boundaries were assumed to be cold at 300 K and black.

3.1. *High coflow air velocity*

Figure 1 shows the predicted distributions of temperature at the highest coflow air flow velocity of $v_A = 77.6$ cm/s under three different gravity levels, i.e. 1 g, 0.5 g, and 0 g, with the maximum temperature indicated in each case. At the normal gravity, Figure 1(a),

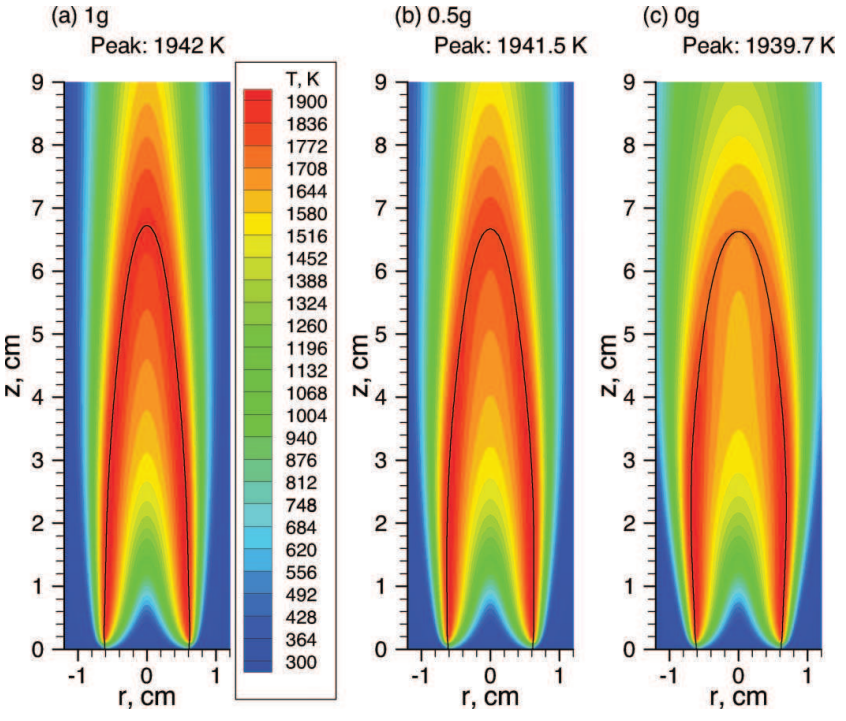

Figure 1. Temperature distributions for $v_A = 77.6$ cm/s. The black curves indicate the stoichiometric mixture fraction (0.05496).

the flame shape is highly elongated owing to buoyancy induced flow acceleration in the streamwise direction, leading to considerable inward radial flow. With decreasing the level of gravity, the flame becomes increasingly wider as a result of reduced radial inflow velocity. The elongated and sharp flame tip in the normal gravity, Figure 1(a), becomes somewhat rounded in microgravity (0 g), Figure 1(c). Since the flame shape is determined by the convection and diffusion processes, the change in the flame shape is associated with the variation in the velocity field. The numerical results indicate that the highest temperatures in the flames (>1900 K) are not at the flame tips, but in the outer annular region lower in the flame at about $z = 0.4$ to 4.0 cm for the normal gravity (1 g) flame, Figure 1 (a), $z = 0.4$ to 3.5 cm for the half gravity (0.5 g) flame, Figure 1(b), and $z = 0.4$ to 3.0 cm for the zero gravity (0 g) flame, Figure 1(c), respectively. Thus, the high-temperature zone becomes shorter when the influence of gravity is increasingly removed. This trend is consistent with the results obtained by Walsh *et al.* [31]. Although the peak flame temperature essentially remains constant at about 1940 K, with a very slight decrease, as the level of gravity is decreased, the temperatures in the upper portion of the flame in the centreline region are actually somewhat significantly reduced, consistent with the shortening of the high-temperature region. The decrease in temperature when the gravity is reduced from 0.5 g to 0 g is larger than those when the gravity is reduced from 1 g to 0.5 g, suggesting that the effect of gravity is highly nonlinear. The reduced buoyancy-induced flow in the streamwise direction with decreasing the gravity level, especially at 0 g, greatly increases the residence time for both soot surface growth and oxidation. At this highest coflow air velocity, the soot formation is significantly enhanced with decreasing gravity (see Figure 6 below). As

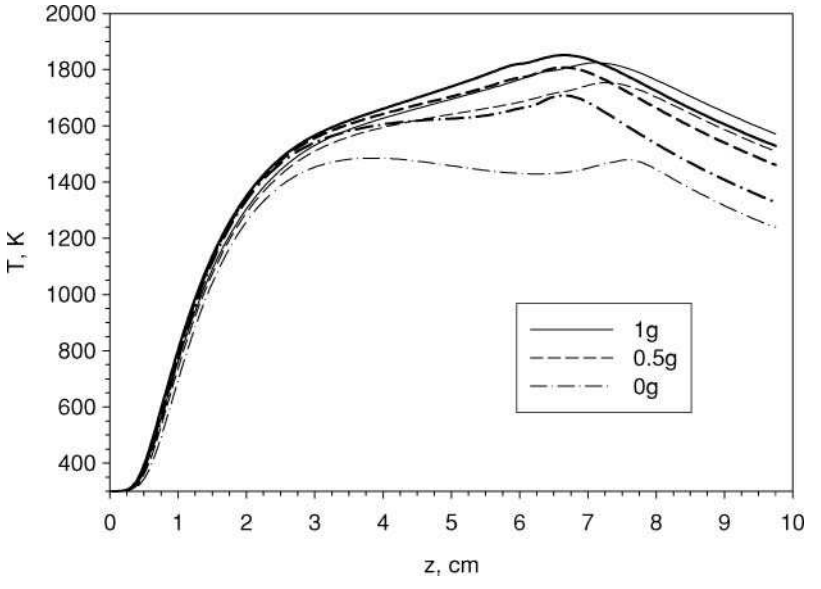

Figure 2. Distributions of temperature along the flame centreline for $v_A = 77.6$ cm/s (thicker black curves) and $v_A = 30$ cm/s (thinner black curves).

a result of both increased soot loading and longer residence times, flame thermal radiation loss is greatly enhanced, which in turn leads to reduced temperature, especially at the upper part of the flame and at 0 g.

The black curves in Figure 1 represent the contour of the stoichiometric mixture fraction. The flame height determined by the location of the stoichiometric mixture fraction on the flame centreline remains more or less constant at 6.7 cm, with only very slight decrease, when the gravity level is reduced from 1 g to 0 g. It is noticed that the centreline location of the stoichiometric mixture fraction is also the location where the temperature peaks on the flame centreline at all three gravity levels.

Figure 2 shows the temperature distributions along the flame centreline under different gravity levels. It is seen that the effects of gravity on flame temperature at this high coflow air velocity are mainly in regions away from the burner exit beyond about $z = 3$ cm. This is because the coflow air in this case has a high momentum to induce a strong radially inward flow in the near burner exit region. At higher streamwise locations ($z > 3$ cm), the centreline temperature decreases with decreasing gravity, which is primarily caused by the enhanced thermal radiation loss discussed above. The enhanced thermal radiation heat loss from the 0 g flame causes the centreline flame temperature to drop significantly beyond about $z = 4$ cm. The increased relative importance of radial heat conduction with decreasing gravity also contributes to the centreline temperature decreases in the upper portion of the flame. The peak centreline temperature at normal gravity reaches about 1851 K, it decreases substantially to about only 1708 K at 0 g.

The axial velocity distributions at the three gravity levels are shown in Figure 3. Note that different color scales are used for each plot in Figure 3 owing to the large variation in the axial velocity. To illustrate the flow directions, the velocity vectors (not scaled to the velocity magnitude) are also shown in Figure 3. The reduced radially inward flow at 0 g is clearly shown. At 1 g and 0.5 g, the axial velocity continues to increase with

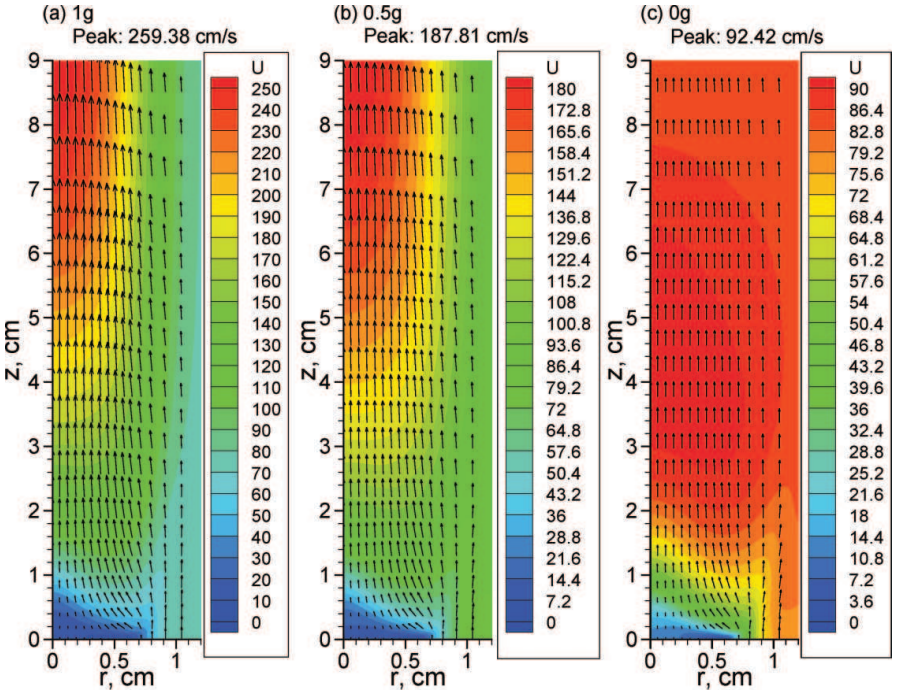

Figure 3. Axial velocity distributions (colour contours, in cm/s) and velocity vectors for $v_A = 77.6$ cm/s.

height owing to gravity acceleration and the radial profile of the axial velocity at a given height in the upper portion of the flame displays is bell-shaped. At 0 g, however, the axial velocity is more or less uniform in both the radial and streamwise directions above about $z = 2$ cm.

The centreline axial velocity distributions are compared in Figure 4. Also plotted in Figure 4 are the theoretical axial velocity under an acceleration rate of $a = 2500$ cm^2/s and 1250 cm^2/s for the normal and half gravity cases, respectively, following Roper *et al.* [43]. The theory predicts a faster increase in the axial velocity in the near burner exit region ($z <$ 1.2 cm) and then a slower increase at higher streamwise locations than the numerical results at both the normal and half gravity cases. Such discrepancy between the numerical results and the simple buoyancy-induced velocity, i.e. $u \propto (az)^{0.5}$, at both the normal and half gravity is qualitatively similar to that between experimentally measured centreline axial velocity and the simple theoretical prediction for buoyancy controlled coflow axisymmetric laminar diffusion flames at normal gravity [42]. In addition, the centreline axial velocities at the normal gravity are also in reasonably good quantitative agreement with the experimental measurements of Santoro *et al.* [42] conducted under similar conditions to the present study (filled circles in Figure 4). Under the present conditions, the flame at the normal and half gravity is buoyancy controlled, judged by the smallness of the modified Froude number ($<\sim 0.1$) defined by Roper [44]. At 0 g, the flame is momentum controlled owing to the absence of buoyancy induced flow acceleration.

The centreline axial velocity distributions shown in Figure 4 indicate a significant reduction in axial velocity with decreasing the level of gravity owing to the loss of buoyancy-induced flow acceleration. The difference increases with the distance above the burner, as the

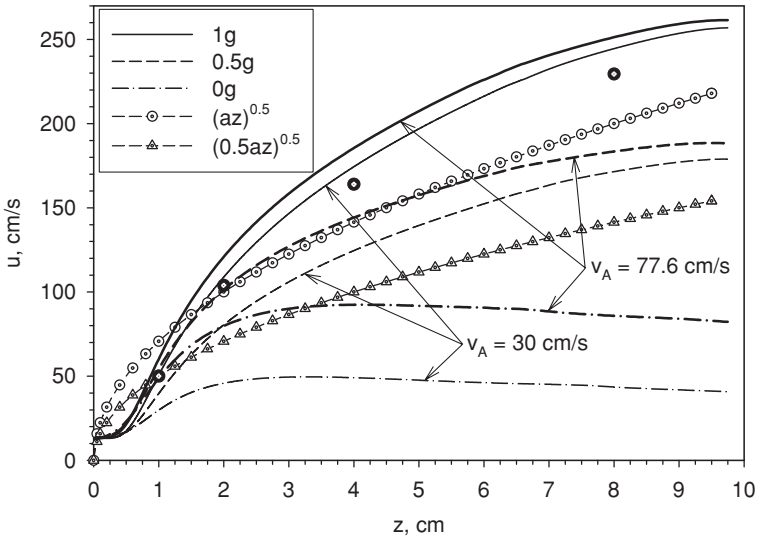

Figure 4. Distributions of axial velocity along the flame centreline for $v_A = 77.6$ and 30 cm/s. The experimental data are from Santoro *et al.* [42] for a laminar ethylene diffusion flame established with an 11.1 mm i.d. fuel pipe and 3.98 and 8.9 cm/s for the fuel and air stream velocity, respectively. The theoretical results were obtained using $a = 2500$ cm/s^2.

buoyancy induced velocity is proportional to the square-root of the distance from the burner exit. Thus, the axial velocities in the normal and half gravity flames increase continuously with the axial height z. While at 0 g, there is no buoyancy-induced flow acceleration, and the transport of combustion products and the supply of fresh air and fuel to the reaction zone reply on the process of molecular diffusion and the coflow air jet momentum. At 0 g the axial velocity peaks around $z = 3.5$ cm in the centreline region and then decays slowly with increasing the flame height. The initial increase in the axial velocity at 0 g is owing to the combined effect of the much higher coflow air velocity (than the fuel jet velocity) and the heat release induced flow acceleration. The subsequent decrease in the axial velocity is also expected owing to the radial diffusion of momentum and the absence of buoyancy induced flow acceleration. The magnitude of axial velocity in the upper portion of the 0 g flame is closely related to the coflow air velocity and this point becomes clear later by examining the results of the lower coflow air velocities presented below.

The decrease in buoyancy-induced acceleration in the vertical direction leads to reduced radial inward flow velocities, Figure 3. As a result, the flame becomes increasingly wider as the level of gravity is reduced, Figure 1. Furthermore, it is clearly seen from Figure 4 that the influence of buoyancy on the centreline axial velocity can be neglected in the near burner region when the axial position z is less than about 0.75 cm. It is also expected that this critical height is affected by the coflow air velocity, i.e. the higher the coflow air velocity, the greater the critical height.

To illustrate the effect of gravity on the characteristic residence time quantitatively, Figure 5 compares the residence time distributions along the flame centreline at the three gravity levels considered. Clearly, the residence time increases with decreasing the gravity level, which is a direct consequence of reduced axial velocity shown in Figures 3 and 4. The initial residence time to travel a short distance above the burner exit for $v_A = 77.6$ cm/s, about 1.5 cm, is almost independent of the gravity level. Owing to the relatively small

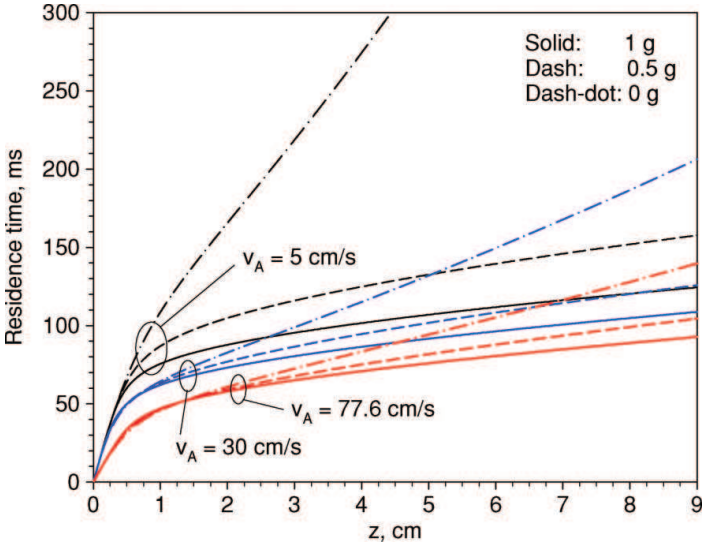

Figure 5. Residence times of a fluid parcel along the flame centreline for $v_A = 77.6$, 30, and 5 cm/s and three gravity levels of 1 g, 0.5 g, and 0 g.

difference in the characteristic residence time between the 1 g and 0.5 g cases, the flame temperature distributions, shown in Figures 1 and 2, and soot volume fraction (shown in Figure 6 below) do not exhibit significant changes, though the relative role of diffusion is enhanced at 0.5 g. As a result of a greater increase in the residence time in 0 g, which enhances thermal radiation, soot formation and oxidation, as well as radial and streamwise diffusion, the flame structure (temperature and species distributions) and soot display a much stronger variation from those at 1 g and 0.5 g. However, the overall effects of gravity on the flame structure and soot field are still relatively small at this highest coflow air velocity compared with those at lower coflow air velocity shown later.

Figure 6 shows the distributions of soot volume fraction at the three gravity levels. It is first observed that the visible flame (owing to soot luminosity) increases slightly, though it becomes wider in the radial direction and sootier (more soot is formed), as the gravity level is decreased. Because of the higher soot volume fraction and the longer residence time at 0 g, the flame emits larger amount of thermal radiation leading to lower temperatures in the upper portion of the flame shown in Figures 1 and 2. The high values of soot volume fraction in each case appear in the annular region. The visible flame diameter in the 0 g flame is greater than that in the normal or the half gravity flame, as a result of reduced radially inward flow. The peak soot volume fraction increases from 0.648 ppm, to 0.836 ppm, and to 1.212 ppm, as the gravity level is decreased from 1 g, to 0.5 g, and 0 g, respectively. The peak soot volume fraction exhibits a stronger increase as the gravity is decreased from 0.5 g to 0 g. The predicted maximum soot volume fraction at 0 g is less than doubled (a factor of 1.87) compared with that at 1 g. Although such an increase in the peak soot volume fraction is in close agreement with that observed from drop tower experiments [14, 15], it should be regarded as a coincidence considering the differences in the operation conditions in terms of the type of fuel, burner size, and coflow air. In our numerical calculations, the burner diameter was about 11 mm and CH_4 was delivered into a coflowing air of 77.6 cm/s velocity. In the drop tower experiments [14, 15], however, the

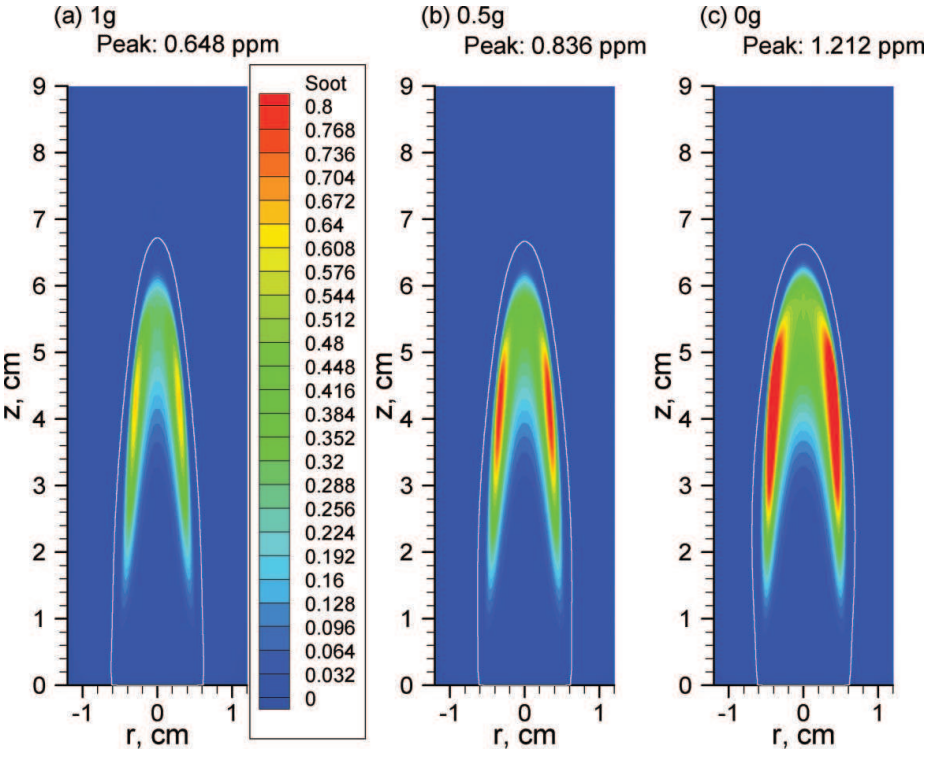

Figure 6. Distributions of soot volume fraction (in ppm) for $v_A = 77.6$ cm/s. The white curves indicate the stoichiometric mixture fraction.

burner diameter was substantially smaller at 1.6 mm and N_2 diluted C_2H_2 was issued into quiescent air. As such, the flame experimentally studied in Refs. 14 and 15 is highly sooting (the peak soot volume fractions are about 8 ppm at 1 g and 16 ppm at 0 g), though its sizes at 1 g and 0 g are significantly smaller than those of this study at the corresponding gravity. Since the overall thermal radiation heat loss is controlled by the flame size, the level of soot loading and the residence times, it is expected that the methane flames studied here have different degrees of radiation heat loss from those of the nitrogen diluted acetylene flames in [14, 15]. It is also worth pointing out that the peak soot volume fraction in a diffusion flame is a result of two competing processes, i.e. surface growth and oxidation. Besides fuel type, they are highly dependent on the fuel flow rate, flame structure, temperature field, and residence time. Given such different operation conditions between our numerical study and those of the experiments [14, 15], the close agreement between the predicted increase in the peak soot volume fraction and that found experimentally is not expected. In fact, as shown later, when the gravity level is reduced from 1 g to 0 g the variation in the peak soot volume fraction is strongly affected by the coflow air velocity. It is clear from the above discussion that the relative variation in the peak soot volume fraction between a non-buoyant flame and its buoyant counterpart depends on flame size and coflow air velocity and it is not meaningful to compare such variations between flames of very different operation conditions. The increase in the soot loading with decreasing gravity is an indication that the residence time effect, which enhances soot formation, plays a greater role than radiation heat loss, which lowers flame temperature and soot formation rate, at this high coflow air velocity.

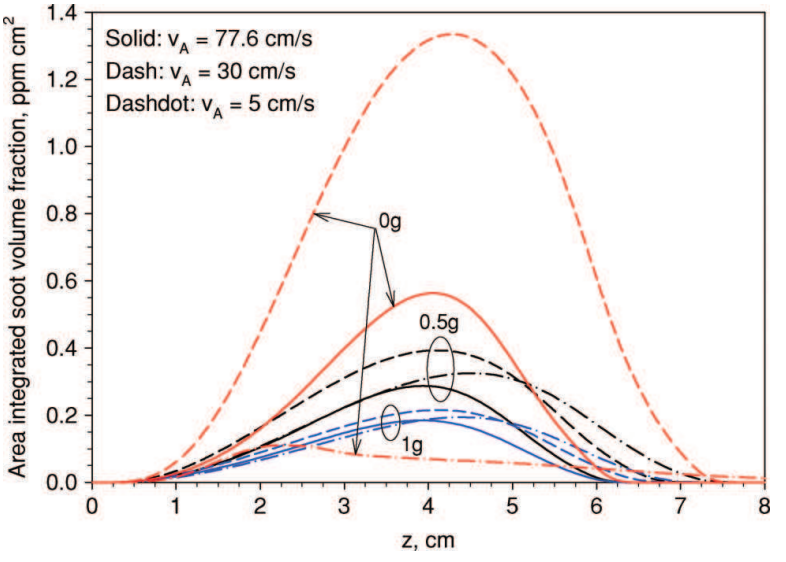

Figure 7. Distributions of flame cross-sectional area integrated soot volume fraction along the flame height for $v_A = 77.6$, 30, and 5 cm/s.

The stoichiometric mixture fraction contours are also shown in Figure 6 to illustrate the relationship between the visible flame shape and that defined by the stoichiometric mixture fraction. It is seen that soot is present just inside the flame sheet defined by the stoichiometric mixture fraction, i.e. soot is fully oxidised on the rich side of the flame. This is because OH, which is the primary soot oxidation species, is present on both sides (rich and lean) of the flame and can fully oxidise soot, especially at 1 g where OH penetrates deeper into the rich side in the flame centreline region. The visible flame height is always shorter than the flame height defined by the stoichiometric mixture fraction under the present conditions for the reason just discussed, with the ratio of the luminous flame height to the stoichiometric one varies from 0.93 at 1 g and 0.5 g to 0.95 at 0 g. The flame heights ratio at 1 g is in reasonably good agreement with that of Mitchell *et al.* [45], who obtained a ratio of 0.9 for a CH_4 diffusion flame of a similar size to our study.

Figure 7 compares the flame cross-sectional area integrated soot volume fraction, $\int_0^\infty 2\pi r f_v dr$, at different gravity levels (see solid lines for $v_A = 77.6$ cm/s). The integrated soot volume fraction increases more significantly than the soot volume fraction itself as the gravity level decreases. This is because the flame becomes not only sootier, but also larger in diameter. It is evident from Figure 7 that the visible flame height (axial location where soot disappears) at $v_A = 77.6$ cm/s (solid lines) increases only very slightly as the gravity is gradually reduced. An examination of the soot nucleation and surface growth rates (not shown) indicates that they are more or less independent of the gravity level in the lower portion of the flame below about $z = 3$ cm. At higher axial locations, especially in the flame centreline region, the nucleation and growth rates at 0 g are actually significantly lower. In other words, the regions of soot nucleation and surface growth become wider but shorter when the influence of gravity is removed. It is therefore believed that the increase in the soot loading with decreasing the gravity level is attributed to the increase in residence times under these conditions. Also the increased soot loading with decreasing the gravity

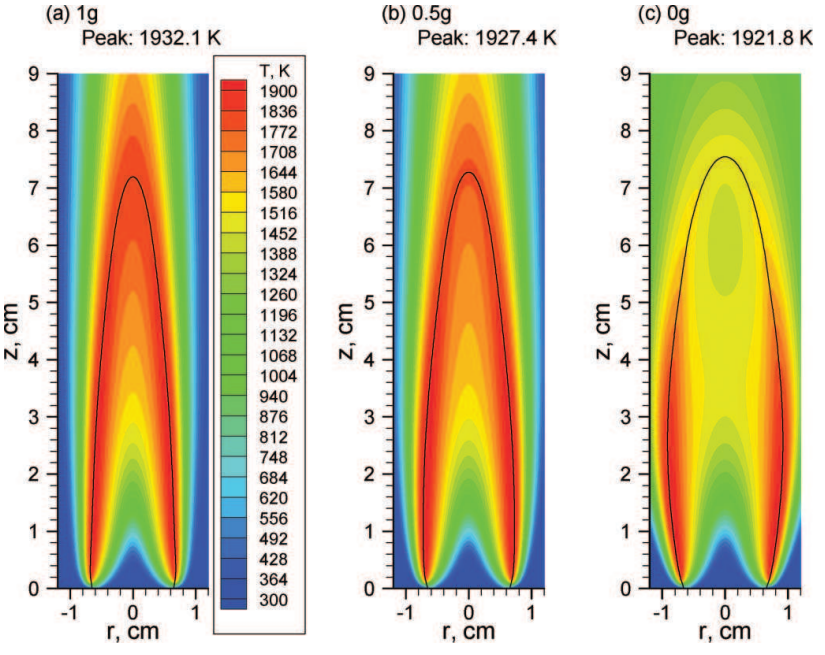

Figure 8. Temperature distributions for $v_A = 30$ cm/s. The black curves indicate the stoichiometric mixture fraction.

levels implies that the prolonged residence times favor soot formation over soot oxidation at this high coflow air velocity.

3.2. *Intermediate coflow air velocity*

Figure 8 shows the predicted distributions of temperature at the intermediate coflow air flow velocity of $v_A = 30$ cm/s under the three gravity levels with the maximum temperature indicated in each case. Again, the stoichiometric mixture fraction contours are plotted to indicate the flame front location. At 1 g, Figure 8(a), the flame shape is again highly elongated similar to the highest coflow air velocity case shown in Figure 1(a) owing to buoyancy induced flow acceleration in the streamwise direction, which leads to significant radially inward flow. Therefore, at normal gravity the effect of coflow air velocity on the general flame shape is insignificant. However, the flame height based on the stoichiometric mixture fraction at 1 g increases from 67 mm to 72 mm as the coflow air velocity is reduced from 77.6 cm/s to 30 cm/s, in qualitative agreement with that observed in the numerical study of Kaplan and Kailasanath [25]. This is attributed to the reduced radially inward flow velocity with decreasing the coflow air velocity. With decreasing the level of gravity, the flame becomes wider and taller as a result of increasingly important role played by the radial and streamwise diffusion. Again, the highest temperatures occur in the outer annular region lower in the flame and the high-temperature zone becomes shorter when the influence of gravity is increasingly removed. The decreases in temperature when the gravity is reduced from 0.5 g to 0 g are larger than those when the gravity is reduced from 1 g to 0.5 g. It is evident from Figure 8(c) that the flame temperatures in the centreline region are significantly reduced at 0 g.

The flame height based on the stoichiometric mixture fraction increases slightly, but more pronounced than that for $v_A = 77.6$ cm/s, with decreasing the gravity. Once again, the flame front on the flame centreline is also the location where the temperature peaks along the flame axis at all three gravity levels investigated.

The temperature distributions along the centreline are compared in Figure 2, where the centreline flame temperature distributions for $v_A = 77.6$ cm/s are also shown for comparison. Again, the effects of gravity on flame temperature at this intermediate coflow air velocity are mainly in regions away from the burner exit beyond about $z = 1.5$ cm. This is because the coflow air at this velocity still carries a relatively high momentum to suppress the radial spread of the flame in the near burner exit region, through the relatively strong radially inward flow. At higher streamwise locations ($z > 1.5$ cm), the centreline temperature decreases with decreasing gravity, which is primarily caused by the enhanced thermal radiation loss and to a much lesser degree the enhanced importance of radial heat conduction. The enhanced thermal radiation heat loss from the 0 g flame causes the centreline flame temperature to drop significantly beyond $z = 3$ cm. It is noticed from Figures 8 and 2 that the centreline temperature at 0 g displays a double peak distribution, a result owing to the significant temperature reduction by enhanced thermal radiation heat loss from soot. It is also noticed from the centreline temperature profile for $v_A = 77.6$ cm/s and 0 g, Figure 2, that there exists a dip between $z = 4.5$ cm and $z = 6.25$ cm. This temperature profile displays a strong similarity to that for $v_A = 30$ cm/s and 0 g, albeit the degree of the dip is smaller and the peak temperature (at the stoichiometric mixture fraction) is much higher. Compared with the temperature distributions at $v_A = 77.6$ cm/s, the centreline temperatures at $v_A = 30$ cm/s peak at a higher axial location at all three gravity levels, Figure 2, consistent with the observation mentioned earlier that the flame becomes taller as the coflow air velocity decreases. There are only relatively small temperature drops at 1 g and 0.5 g as the coflow air velocity is decreased. However, at 0 g the peak temperature on the flame centreline drops significantly from 1708 K at $v_A = 77.6$ cm/s to 1485 K at $v_A = 30$ cm/s.

The axial velocity distributions for $v_A = 30$ cm/s are compared in Figure 9. Velocity vectors are also plotted in this figure to illustrate the flow directions. Again different color scales are used at different gravity levels owing to the large variation in the velocity magnitude. The distributions of axial velocity along the flame centreline are shown in Figure 4. The flame at the normal and half gravity is still buoyancy controlled. This is confirmed by the observations that the axial velocity distributions at 1 g and 0.5 g remain somewhat weakly dependent on the coflow air velocity, Figures 4. At 0 g, the flame is momentum controlled owing to the absence of buoyancy induced flow acceleration. Consequently, the coflow air velocity plays an important role. This is highlighted in the numerical results shown in Figure 4 that the centreline axial velocity is reduced by almost a factor of 2 at 0 g (dash-dot lines) when the coflow velocity is reduced from 77.6 cm/s to 30 cm/s.

The centreline axial velocity distributions shown in Figure 9 are qualitatively similar to those shown in Figure 3 for $v_A = 77.6$ cm/s and the discussions made there are also relevant to Figure 9. In particular, the radially inward flow is weakened as the gravity leave is lowered and the axial velocity profile becomes more uniform. As a result, the flame becomes wider and taller. The effect of coflow air velocity becomes more significant with decreasing the gravity level, especially when the gravity is removed. In this case (0 g), the transport of combustion products and the supply of fresh air and fuel to the reaction zone reply on the process of molecular diffusion and the coflow air jet momentum, as the buoyancy induced convection is absent. With reduced coflow air velocity and the absence of gravity, the diffusion of heat and mass in both the radial and streamwise directions plays a greater role.

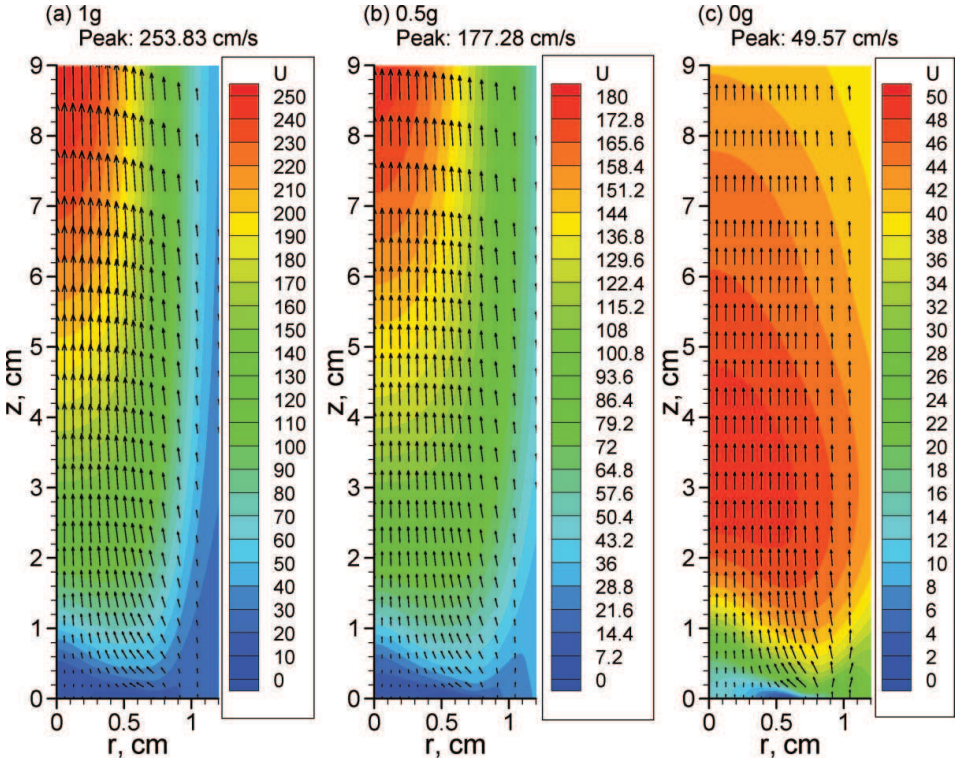

Figure 9. Axial velocity distributions (colour contours, in cm/s) and velocity vectors for $v_A = 30$ cm/s.

To illustrate the effects of gravity level and coflow air velocity on the characteristic residence time quantitatively, the residence time distributions along the flame centreline at the three gravity levels considered for $v_A = 30$ cm/s (blue lines) are compared in Figure 5. As anticipated from the centreline axial velocity distributions shown in Figure 9, the characteristics residence times at 1 g and 0.5 g do not differ very significantly at this coflow air velocity. At 0 g, the characteristic residence time starts to deviate significantly from those at 0.5 g and 1 g beyond about $z = 1.5$ cm. Such an increase in the residence time is primarily responsible for the enhanced soot formation shown below.

Figure 10 shows the distributions of soot volume fraction at the three gravity levels. With decreasing the gravity level the visible flame becomes more significantly taller and sootier than that at $v_A = 77.6$ cm/s. Again, the visible flame is enveloped just inside the flame sheet, especially at 0 g shown in Figure 10(c), owing to complete oxidation of soot by OH. It is noticed again that the visible flame tip is getting closer to the flame tip as the gravity is reduced. The effect of gravity on the visible flame and soot concentration is more pronounced at this intermediate coflow air velocity than that at the higher air velocity. As a result of higher soot volume fraction and longer residence times at 0 g, soot emits larger amount of thermal radiation in microgravity leading to much lower temperatures in the upper portion of the flame shown in Figures 2 and 8. The maximum values of soot volume fraction in each case again appear in the annular region. The peak soot volume fraction increases from 0.7 ppm, to 0.986 ppm, and to 1.87 ppm, as the gravity level is decreased from 1 g, to 0.5 g, and then 0 g, respectively. The peak soot volume fraction

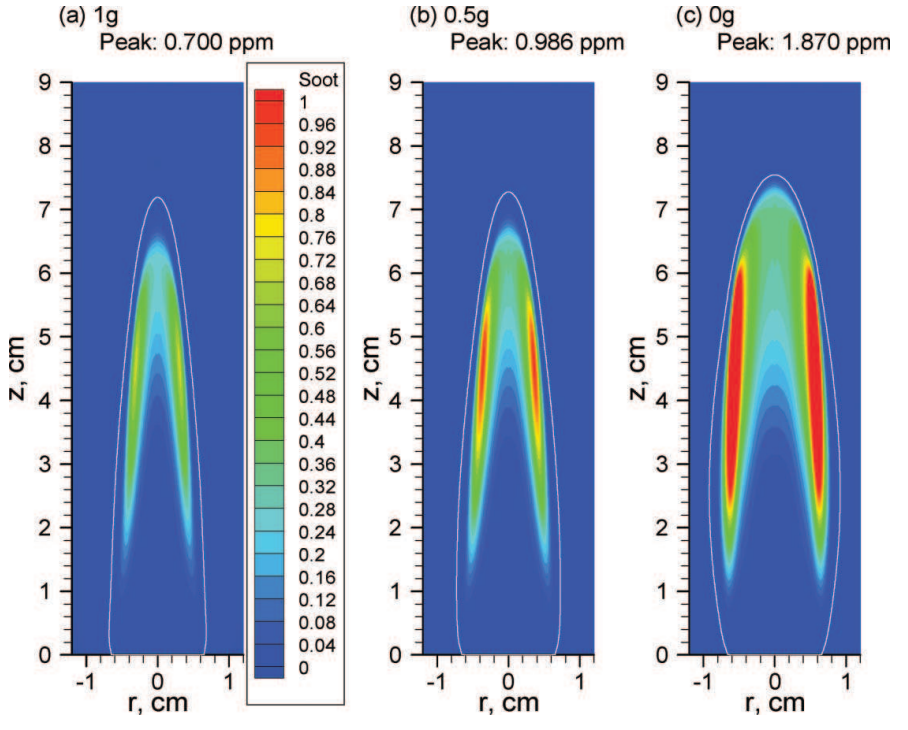

Figure 10. Distributions of soot volume fraction (in ppm) for $v_A = 30$ cm/s. The white curves indicate the stoichiometric mixture fraction.

exhibits a stronger increase with decreasing gravity level compared with the higher coflow air velocity case. The predicted maximum soot volume fraction under 0 g is more than double that under 1 g (a factor of 2.7).

The flame cross-sectional area integrated soot volume fractions, $\int_0^\infty 2\pi r f_v dr$, at different gravity levels are compared in Figure 7. As the flame becomes sootier and wider with decreasing the gravity level, the integrated soot volume fraction increases much more significantly than soot volume fraction itself. The gravity effect on soot formation at $v_A = 30$ cm/s is much stronger than that at $v_A = 77.6$ cm/s. The increase in the visible flame height, where soot disappears on the flame centreline, with decreasing the gravity level is also evident. Once again, the increase in soot loading with decreasing the gravity level is attributed to the increase in residence times and suppressed radially inward flow. The latter leads to a taller and wider flame. Like the case of $v_A = 77.6$ cm/s, the enhanced soot production at $v_A = 30$ cm/s is again an indication that the residence time effect to promote soot formation is dominant over the increased role of radiation heat loss, which is to reduce soot formation through the temperature effect.

3.3. *Low coflow air velocity*

Figure 11 shows the predicted distributions of temperature under the lowest coflow air flow velocity of $v_A = 5$ cm/s at the three gravity levels with the maximum temperature indicated in each case. Again the stoichiometric mixture fraction contours are plotted as black curves. It is noticed that Figure 11(c) is generated over a wider range in the radial

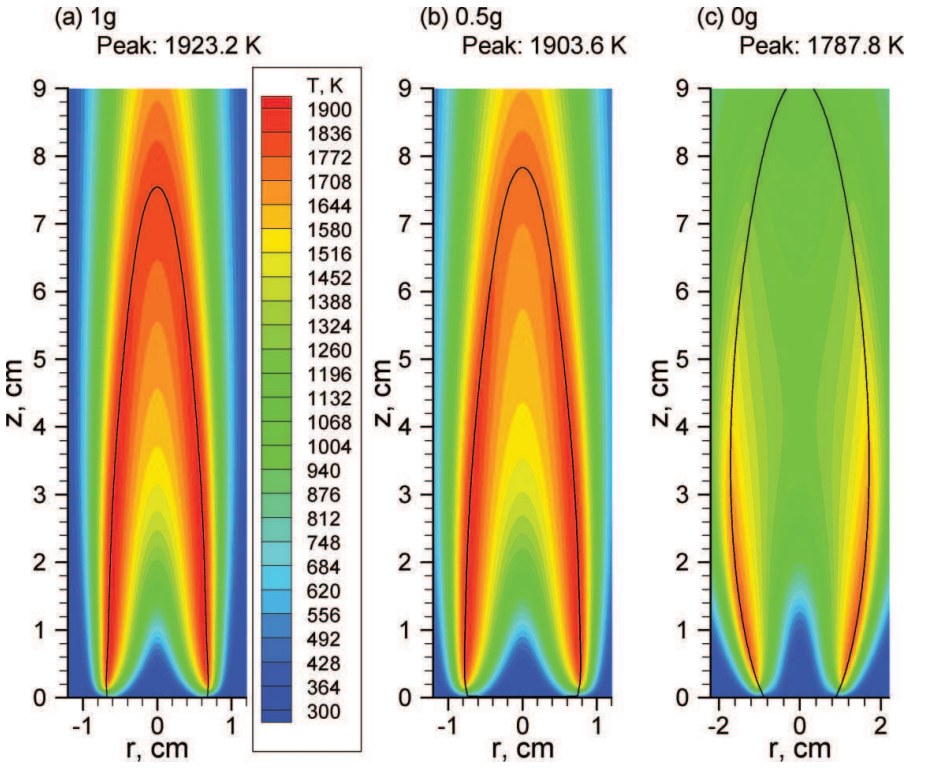

Figure 11. Temperature distributions for $v_A = 5$ cm/s. The black curves indicate the stoichiometric mixture fraction.

direction (−2.2 cm, 2.2 cm) than previous color plots and Figures 11(a) and 11(b), since the flame becomes much wider at this lowest coflow air velocity and 0 g. The flame height at any given gravity level becomes significantly taller than its counterpart at higher coflow air velocities, especially at 0 g. In contrast to the results shown in Figures 1 and 8, where the peak flame temperature decreases only very slightly to somewhat modest with decreasing the gravity level, the peak flame temperature now decreases significantly from 1923.2 K at 1 g, to 1903.6 K at 0.5 g, and further to 1787.8 K at 0 g. Thus, the coflow air velocity has a very strong influence on the flame temperature and structure, especially at microgravity. Even at the normal gravity (1 g), the peak flame temperature is reduced by about 20 K when the coflow air velocity is decreased from 77.6 cm/s to 5 cm/s. To our knowledge, the decrease of the peak flame temperature with decreasing the coflow air velocity at normal gravity has not been reported previously. Such decrease in the peak flame temperature, which occurs in the annular region and in the lower portion of the flame, may be primarily attributed to the increase in residence time, which enhances heat loss from the high temperature region through thermal radiation.

Besides the significant decrease in the peak flame temperature with decreasing the gravity level, there is even more drastic reduction in temperature in the centreline region at 0 g, Figure 11(c). To quantitatively illustrate such reduction, Figure 12 compares the flame centreline temperature distributions at the three gravity levels. To provide a direct comparison, the centreline temperature distributions at the higher coflow air velocity of $v_A = 30$ cm/s are also plotted as grey curves. At the higher coflow air velocity, the centreline

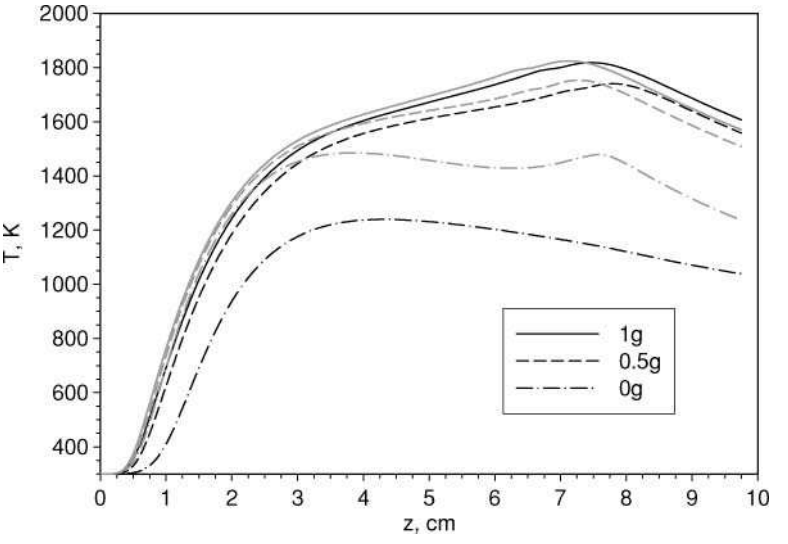

Figure 12. Distributions of temperature along the flame centreline for $v_A = 5$ cm/s (black curves). The corresponding results for $v_A = 30$ cm/s are plotted as grey curves for comparison.

temperature distribution is weakly dependent on the gravity level at axial locations below about $z = 1.5$ cm, Figure 12. At this lowest coflow air velocity of $v_A = 5$ cm/s, however, the centreline temperature decreases with decreasing the gravity level right above the burner exit, especially at 0 g. These results clearly demonstrate the importance of coflow air to the structure of laminar diffusion flame at microgravity. At 1 g and 0.5 g, the decrease in the coflow air velocity from 30 cm/s to 5 cm/s causes only a slight decrease in the centreline temperature with the peak temperature occurs at a slightly higher axial location. At 0 g, the decrease of the coflow air velocity from 30 cm/s to 5 cm/s causes the centreline temperatures drop drastically by more than 200 K over a large portion of the flame and the peak centreline temperature to only 1250 K. Such a drastic decrease in the centreline temperatures at 0 g is again associated with the significant increase in the residence time (shown later), which allows much greater heat loss from the flame primarily through thermal radiation. From the results shown in Figures 2 and 12 it is reasonable to postulate that the centreline temperatures would further decrease to such levels that complete quenching occurs in the centreline region if the coflow air velocity is further reduced, i.e. close to the situation of quiescent air. Therefore, the present numerical results tend to provide some support to the explanations of Urban *et al.* [16] to their experimental observations that soot is contained within a narrow annular ring, i.e. the centreline region is soot free. They argued that as a result of enhanced continuum radiation heat loss from soot at 0 g the temperatures in the centreline region are so low that the fuel does not decompose and the subsequent soot formation processes do not occur. Their argument implies that unburned hydrocarbons emit from tip-opened flames at 0 g. In fact, quenching occurs in the centreline region of the 0 g flame at $v_A = 5$ cm/s as shown later.

The effects of gravity level on the axial velocity distribution are compared in Figure 13. Also plotted in Figure 13 are velocity vectors (not scaled in magnitude) to illustrate the flow directions. Owing to the much wider flame diameter at 0 g, Figure 13(c) is plotted over a larger radial range than Figures 13(a) and 13(b). The distributions of axial velocity at 1 g and 0.5 g are very similar to those shown earlier at higher coflow air velocities, Figures 3

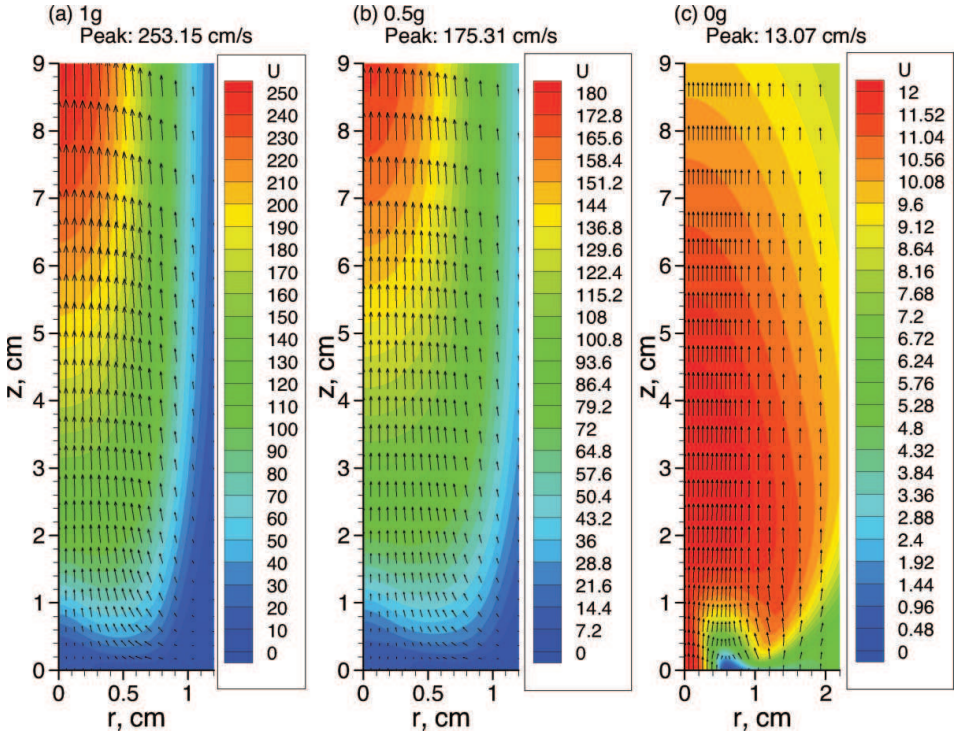

Figure 13. Axial velocity distributions (colour contours, in cm/s) and velocity vectors for $v_A =$ 5 cm/s.

and 9, with their magnitudes being only slightly lower than their counterparts at the higher coflow air velocity. This is actually expected since the flame is buoyancy controlled at 1 g and 0.5 g and the effect of coflow air velocity quickly vanishes with increasing distance from the burner exit. At 0 g, Figure 13 (c), the distribution of axial velocity is also qualitatively similar to those shown in Figures 3(c) and 9(c), albeit the magnitude is lower and the peak axial velocity occurs at a lower height. It is evident from Figure 13 that the radially inward flow weakens with decreasing the gravity level. This is the reason why the flame becomes taller and wider with decreasing the gravity level.

A closer examination of the velocity vectors shown in Figure 13(c) indicates that there exists a region above the fuel stream exit where there is radially outward flow, instead of inward one. To better show the effect of the coflow air velocity on the radial velocity at 0 g, Figure 14 compares the radial velocity distributions at the three different coflow air velocities. Also plotted in this figure are the stoichiometric mixture fraction (dash-dot black curves) and zero radial velocity contours (solid black curves). It is first observed from Figure 14 that the magnitude of radial velocity decreases with decreasing the coflow air velocity, which is closely associated with the increases of the flame height. Owing to the absence of buoyancy induced flow acceleration at 0 g, these radial velocity distributions are very different from those at 1 g and 0.5 g (not shown) where the radial velocities are almost everywhere negative (radially inward flow). The radial velocity distributions at 0 g, however, display three different regions in terms of the sign of the radial velocity. In the cases of $v_A = 77.6$ cm/s and $v_A = 30$ cm/s, Figures 14(a) and 14(b), the radial velocity in the centreline region is largely negative (inward flow) while it becomes positive (outward

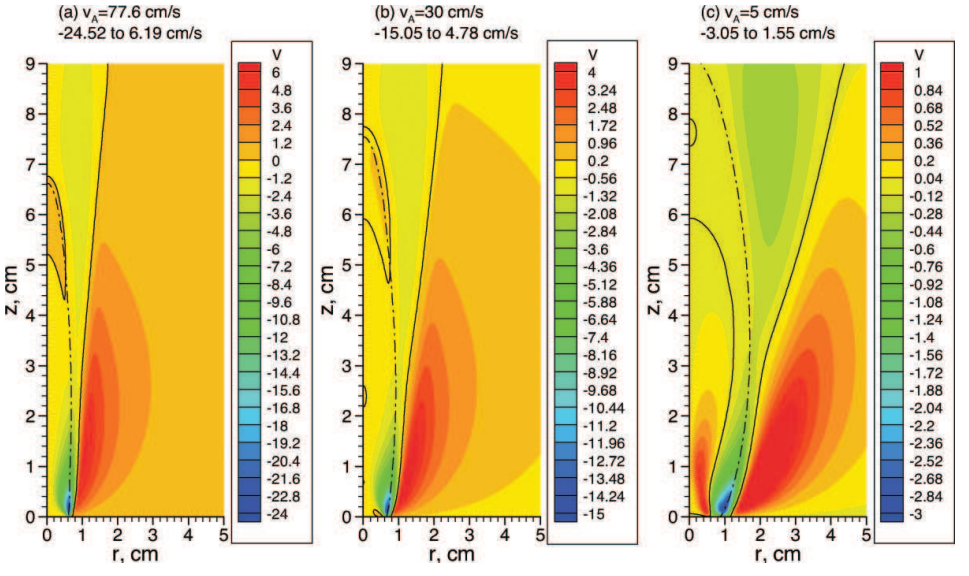

Figure 14. Radial velocity distributions (in cm/s) at 0 g and the three different coflow air velocities.

flow) at larger radial distance. These two regions are separately by the nearly vertical solid black line. In the centreline region, there exists a small region almost just below the flame tip where the radial velocity is positive. However, the magnitudes of the radial velocity in this region are very low (less than 0.4 cm/s at both coflow air velocities). For $v_A =$ 5 cm/s, Figure 14(c), where the coflow air velocity is lower than the mean fuel jet velocity of 6.5 cm/s, the radial velocity in the centreline region up to $z = 6$ cm is actually positive (outward). The region enveloped by the two solid black lines has negative radial velocity components where the flow is radially inward. Outside this region at larger radial distances, the radial velocity components are positive again. Since the structure of a laminar diffusion flame is determined to a large extent by the flow field, it is not surprising to see the large variation in the flame shape at 0 g and 5 cm/s coflow air velocity compared with those at other conditions.

At 0 g, after some slight flow acceleration owing to heat release, the axial velocity decays rather slowly. These behaviours are well illustrated in Figure 15, where the axial velocity distributions along the flame centreline are plotted. To illustrate the effect of the coflow air velocity on the centreline axial velocity distributions, the axial velocity distributions at $v_A = 30$ cm/s are also shown in Figure 15 as grey lines. The relative small effect of the coflow air velocity on the axial velocity distributions at 1 g (solid lines) and 0.5 g (dashed lines) is evident. At 0 g (dash-dot lines), however, such effect is very significant. At the lowest coflow air velocity of $v_A = 5$ cm/s, the axial velocity starts to display dependence on the gravity level almost immediately above the burner exit. This is because of the enhanced radial diffusion of the fuel jet momentum as the coflow air velocity is further reduced from 30 cm/s to 5 cm/s. It is noticed that the latter is lowered than the mean fuel jet velocity of 6.5 cm/s.

With the significant decrease in the axial velocity at 0 g, it is expected that the residence time should be much longer at 0 g and $v_A = 5$ cm/s. This is quantitatively illustrated in Figure 5, where the residence time distributions along the flame centreline at all three coflow air velocities are shown. Although the increase in the residence time with decreasing the

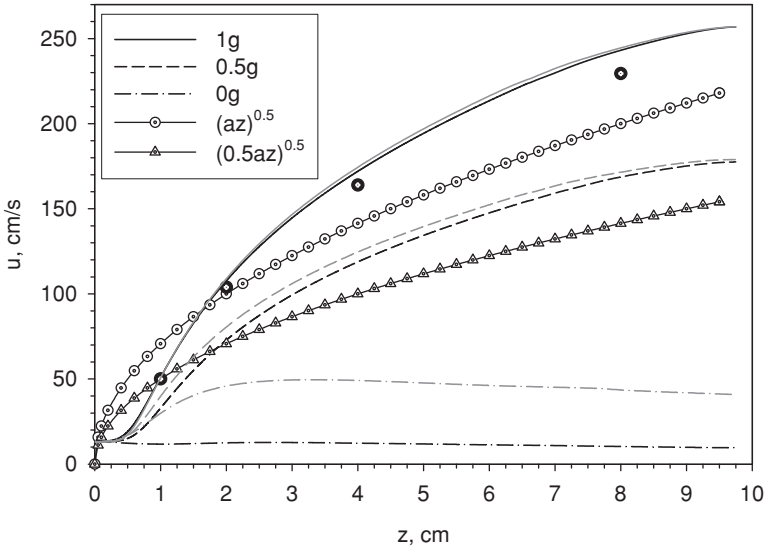

Figure 15. Distributions of axial velocity along the flame centreline for $v_A = 5$ cm/s (black curves). The corresponding axial velocity for $v_A = 30$ cm/s (grey curves) are also plotted for comparison. The experimental data are from Santoro *et al.* [42] for a laminar ethylene diffusion flame established with an 11.1 mm i.d. fuel pipe and 3.98 and 8.9 cm/s for the fuel and air stream velocity, respectively. The theoretical results were obtained using $a = 2500$ cm/s^2.

coflow air velocity at 1 g and 0.5 g is moderate, the increase is quite drastic at 0 g by more than a factor of 3 compared with that of 0 g and $v_A = 30$ cm/s at the flame tip as a result of the much lower axial velocities.

Soot volume fraction distributions at the three gravity levels are shown in Figure 16, where the stoichiometric mixture fraction contours are also plotted as white curves. Note that Figure 16(c) is plotted over a wider radial range than Figures 16(a) and 16(b) and using a different colour scale owing to its much lower soot volume fractions. As in the cases of the higher coflow air velocity shown in Figures 6 and 10, except the 0 g case shown in Figure 16(c), where there is a gap between the luminous flame boundary and the flame sheet between about $z = 3$ and 8 cm and soot escapes the flame tip, the outer radial boundary of the luminous region is just inside the flame sheet. This is in agreement with the finding of Urban *et al.* [16]. At a given level of gravity, the visible flame height increases as the coflow air velocity decreases; however, the peak soot volume fraction actually maximises at the intermediate coflow air velocity, Figures 6, 10 and 16. Such results may be attributed to the two competing effects of reducing the coflow air velocity on soot formation, which results in prolonged residence times: one is to enhance soot formation, the other is to suppress soot formation through lowered flame temperatures associated with increased amount of thermal radiation heat loss. The former is dominant when the coflow air velocity is decreased from 77.6 to 30 cm/s; however, the situation is reversed when the coflow air velocity is further decreased from 30 to 5 cm/s.

At the lowest coflow air velocity considered, the most interesting and unexpected results are those at 0 g shown in Figure 16(c), where the peak soot volume fraction is much lower and the flame emits soot from its tip. At 0 g, the soot volume fraction distribution, Figure 16(c), forms a sharp contrast to those under other conditions of coflow air velocity and gravity level in terms of the level of soot concentration and the shape of the luminous region.

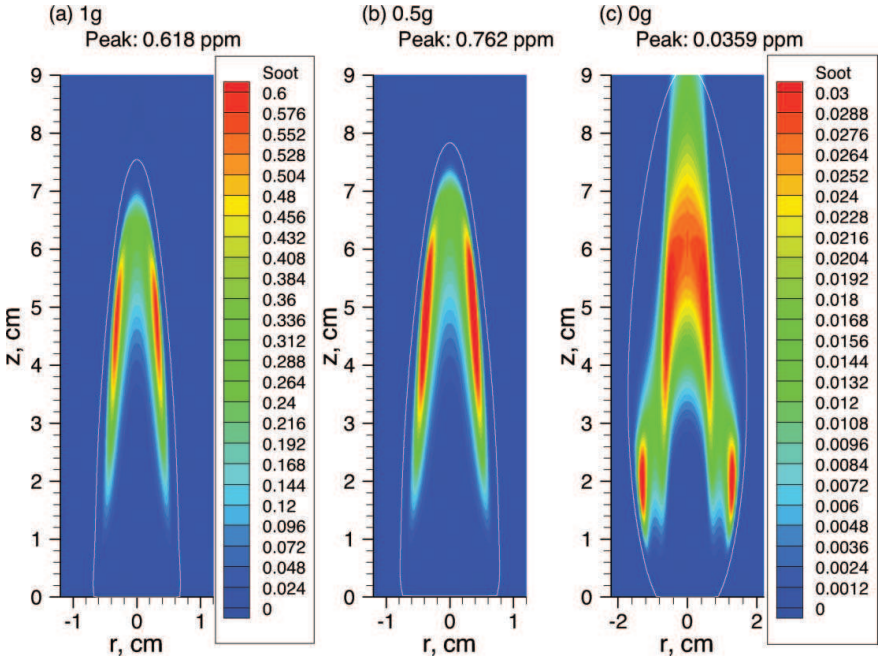

Figure 16. Distributions of soot volume fraction (in ppm) for $v_A = 5$ cm/s. The 1 g and 0.5 g cases use the same colour scales. The white curves indicate the stoichiometric mixture fraction.

Although the present numerical results indicate emission of soot from the centreline region, it is not clear if such a numerically predicted phenomenon corresponds to the blunt flame tip and tip-opening phenomenon observed experimentally [7, 12, 15, 16] owing to the large difference in the size of the flames between this study and those experimental ones. Nevertheless, the results shown in Figure 16(c) are of interest and deserve further numerical and experimental investigations.

The much lower soot concentration shown in Figure 16(c) can be attributed to the much greater radiation heat loss as a result of the much larger flame size and much longer residence time. Consequently, the temperatures are much lower, especially in the centreline region where soot nucleation and growth rates are very low. Such low nucleation and growth rates in the centreline region result in the sooting region along the flame centreline. The combination of a much larger flame size and a much longer residence time affects soot formation and oxidation in a rather complicated way. On one hand, longer residence times are beneficial to soot surface growth. On the other hand, however, they also prompt radiation heat loss, which in turn lowers flame temperature and thus the soot nucleation and growth rates. Therefore, longer residence times enhance two competing processes to soot formation. Our numerical results suggest that at sufficiently high coflow air velocity (30 and 77.6 cm/s) a moderate increase in the residence time by reducing the gravity level favours soot formation enhancement over reduction through reduced temperatures via greater radiation heat loss, i.e. soot loading increases with decreasing the gravity level. This situation is different when the coflow air velocity is low enough, e.g., at 5 cm/s, where soot formation is greatly suppressed at 0 g owing to decreased temperatures, as a result of much greater radiation heat loss through an enlarged flame size and prolonged residence times. Although this point has already made earlier, we like to reiterate it owing to its importance

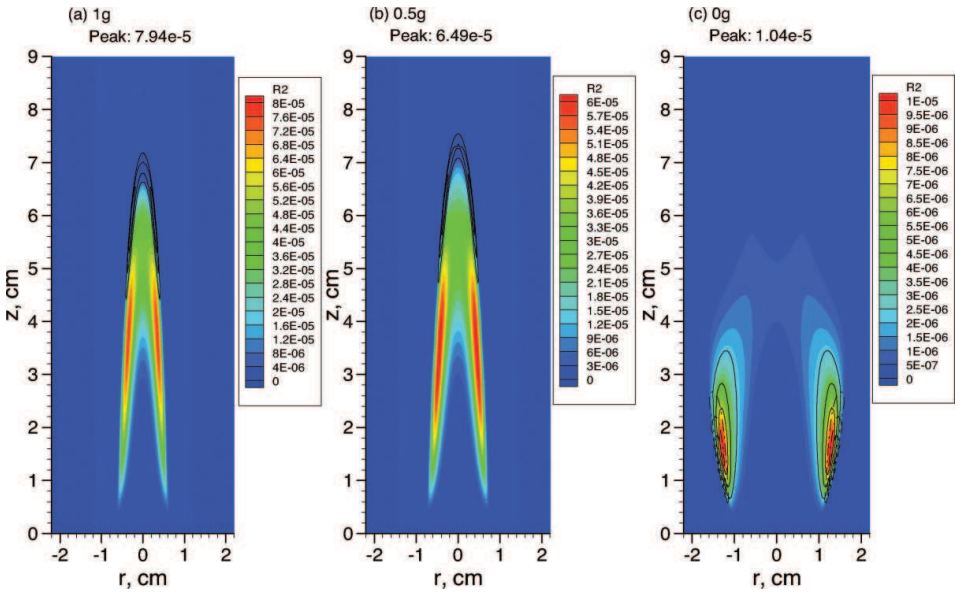

Figure 17. Distributions of soot surface growth rate (g cm^{-3} s^{-1}) for $v_A = 5$ cm/s.The lines in (a) and (b) represent regions of OH oxidation and lines in (c) represent O_2 oxidation.

in understanding the flame structure and soot formation characteristics in microgravity. It is interesting to notice that the decrease in soot loading with increased residence times numerically predicted here is in qualitative agreement with the experimental observations of Legros *et al.* [20] and Fuentes *et al.* [21].

The cross-sectional area integrated soot volume fractions at $v_A = 5$ cm/s are also compared in Figure 7. The levels of integrated soot at 1 g and 0.5 g are similar to those at higher coflow air velocities, albeit the visible flame is taller. However, the integrated soot volume fraction at 0 g is much lower than those at higher coflow air velocities. The escape of soot from the flame tip is also evident from this figure, as the integrated soot volume fraction remains at a small value even at the top boundary.

To gain further insights into the effects of gravity and coflow air velocity on the flame structure and soot formation, the locations of the dominant process for soot production (surface growth) and destruction (oxidation by OH or O_2) were analysed. It was found that in general soot surface growth occurs in the lower portion of the flame while soot is primarily oxidised by OH that occurs in the upper portion of the flame. These features are depicted in Figure 17 at the three gravity levels and at the coflow air velocity of 5 cm/s. In this figure, the color contours represent the soot surface growth rate distributions. The black lines in Figures 17(a) and 17(b) represent the soot oxidation zone by OH at 1 g and 0.5 g, respectively, and the soot oxidation by O_2 in the case of 0 g, Figure 17(c). The soot formation and oxidation regions shown in Figures 17(a) and 17(b) are typically expected in axisymmetric coflow diffusion flames and are also qualitatively similar to those at the two higher coflow air velocities even at 0 g. The soot formation and oxidation regions shown in Figure 17(c) display three major differences from those at other conditions of gravity and coflow air velocity. First, the species primarily responsible for soot oxidation is not OH or O, but O_2. Second, regions of soot growth and oxidation by O_2 overlap more substantially than those in other cases. Third, soot oxidation rates by O, OH, and O_2 all peak

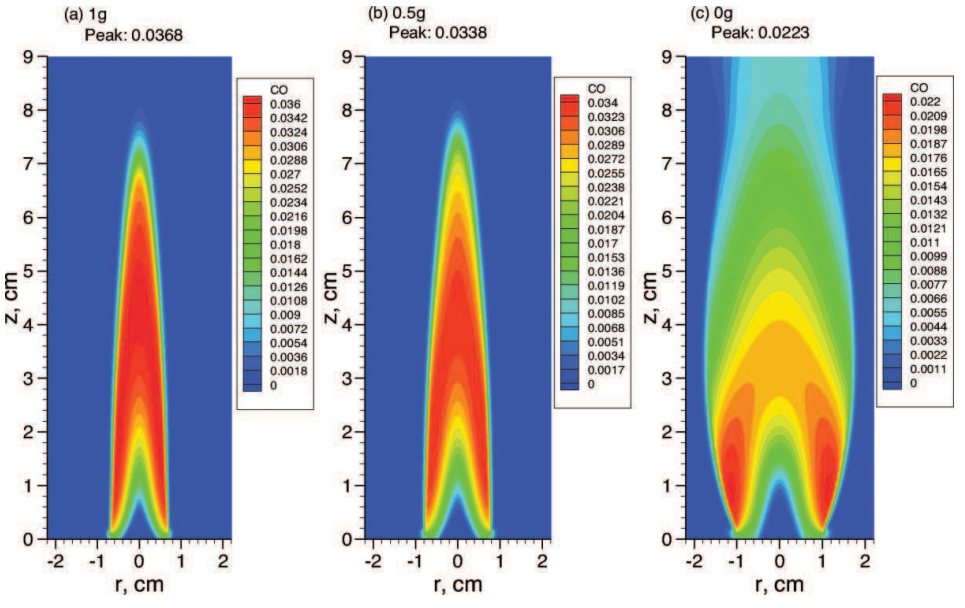

Figure 18. Distributions of CO mass fraction for $v_A = 5$ cm/s.

in the early stage of soot formation in the annular region (between about$z = 1$ and 2.5 cm, results of O and OH oxidation are not shown), instead of occurring near the flame tip in the centreline region. The overlap of soot growth and oxidation regions is clearly another reason for the low soot volume fractions found in the microgravity flame at $v_A = 5$ cm/s, besides the residence time argument discussed above. The reason for the overlap of soot growth and oxidation regions in this flame lies in the flow field. Owing to their very small size, soot particles follow the local flow velocity with only a very small modification by thermophoresis. In all other cases considered, the pathlines originating from the fuel stream or in the immediate region just outside the fuel pipe converge towards the flame centreline either owing to buoyancy-induced flow acceleration or under the momentum of the higher coflow air velocity. As a result, at the normal and the half gravity or when the coflow air velocity is higher, soot particles formed low in the flame are convected towards the flame centreline region to avoid being contacted with the major soot oxidising species, such as O and OH, albeit experiencing slight oxidation by O_2 leaked through the burner rim. Under these scenarios, soot particles go through the fuel-rich region for some extended period time for growth before they are oxidised by O and OH at higher axial locations. At the lowest coflow air velocity considered and without buoyancy-induced flow acceleration (0 g), the pathlines originating from the fuel stream move almost straight upward with a slight radially outward motion. As such, soot nucleation and growth regions overlap with soot oxidation regions, leading to another cause for reduced soot volume fractions, besides the reason of the enhanced thermal radiation heat loss.

The emission of soot from the flame tip at 0 g shown in Figure 16(c) is associated with the incomplete combustion or partial quenching of the flame in the centreline region. This point is further demonstrated in Figure 18 where the distributions of CO mass fraction are plotted. It is evident that at 0 g, Figure 18(c), the flame emits unburned CO and also other hydrocarbon species (not shown).

The potential effect of the thermophoretic velocity of soot on soot volume fraction distribution at 0 g was assessed by analysing the thermophoretic velocities in both the streamwise and the radial directions at $v_A = 5$ cm/s. Our numerical results indicate that radial thermophoretic velocities of soot are much higher than those in the streamwise direction, owing to the larger temperature gradients in the radial direction. However, the radial thermophoretic velocities in the sooting region are always less than 0.5 cm/s. Such magnitude of soot thermophoretic velocity is in agreement with the estimate of Konsur *et al.* [14]. The radial transport of soot by thermophoresis from the annular high soot concentration ring towards the cooler centreline region is likely to be negligible, as suspected by Konsur *et al.* [14]. To further confirm this point, numerical calculations at 0 g and the lowest coflow air velocity were conducted by reducing the magnitude of soot thermophoretic velocities by a factor of 2. Such a reduction in the thermophoretic velocity results in only about half percent increase in the peak soot volume fraction. Therefore, thermophoresis indeed has negligible effect on soot formation in microgravity. Such finding is not surprising owing to much lower temperature gradient in microgravity flames. This conclusion also holds at normal gravity owing to the strong buoyancy-induced convections, albeit temperature gradients are quite high.

Based on the numerical results presented so far, it is reasonable to speculate that the flame at 0 g could become much cooler and less sooting with a further decrease in the coflow air velocity. It is also plausible that a diffusion flame can experience radiation-induced self-extinguishment when the burner diameter exceeds a critical value for a given fuel flow rate at 0 g when the coflow air velocity is sufficiently low. In fact, even at $v_A = 5$ cm/s and at 0 g the flame experiences significant incomplete combustion as indicated by the emission of CO shown in Figure 18(c) and other hydrocarbon species. A larger diameter of the fuel nozzle implies slower fuel exit velocity and longer residence times. Such conjecture of large diffusion flame extinguishment at microgravity based on the present numerical results has yet to be verified by experiments. Although numerous experiments have been conducted on the flame structure and soot formation in laminar diffusion flames at microgravity, the possible self-extinction of large diffusion flames at 0 g has not been observed. This is likely because the existing microgravity experiments were carried out using either very small fuel nozzles less than 3 mm in diameter in drop-towers, e.g. [10,11], or relatively large fuel nozzles in aircrafts flying parabolic trajectories where the gravity levels are still relatively high at about 0.01 g [9]. However, the experimentally observed and numerically predicted phenomenon of radiation-induced counterflow diffusion flame extinction at sufficiently low stretch [46] lends a sound support to the conjecture that there is a critical fuel nozzle diameter for a given fuel flow rate beyond which the diffusion flame in microgravity and quiescent air experiences radiation-induced extinction.

3.4. *The importance of thermal radiation heat transfer in microgravity*

Some interesting phenomena numerically predicted in this study that are not normally observed in laminar coflow diffusion flames at earth gravity, such as the double peak flame centreline temperature distribution shown in Figures 2 and Figure 8(c) under 0 g and $v_A = 30$ cm/s and the much lower soot loading with soot emission from the flame tip shown in Figure 16(c) under 0 g and $v_A = 5$ cm/s , are explained in terms of the enhanced thermal radiation heat loss associated with the larger flame size and prolonged residence times. To unambiguously demonstrate that thermal radiation heat transfer is indeed the mechanism responsible for these phenomena, addition numerical calculations were conducted for the flames at the intermediate and the low coflow air velocity at 0 g with the thermal radiation

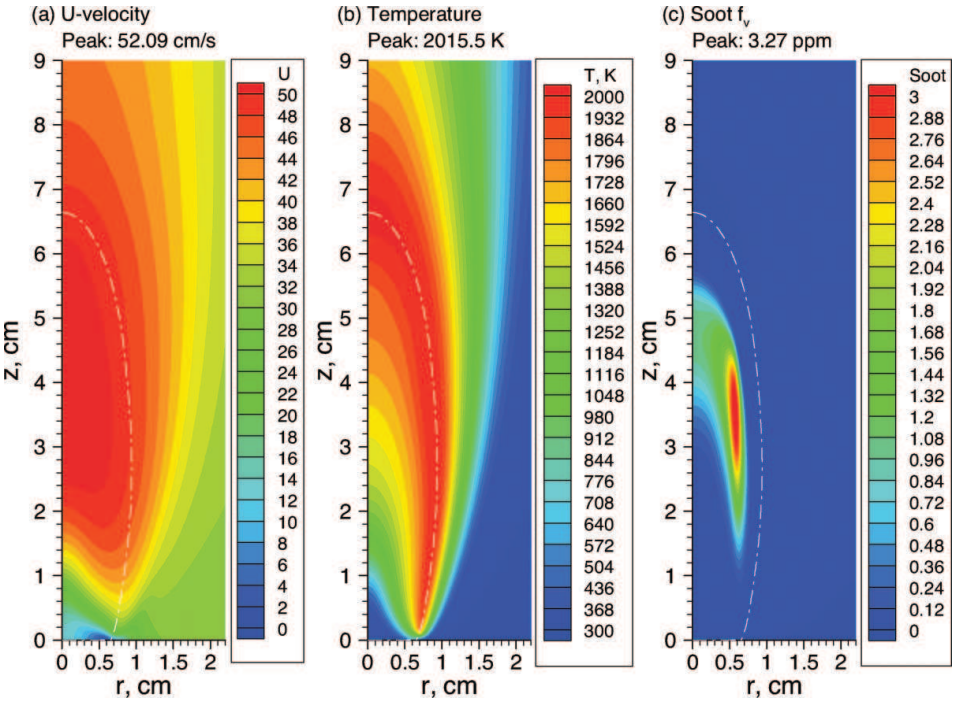

Figure 19. Distributions of axial velocity (in cm/s), temperature, and soot volume fraction (in ppm) at 0 g and $v_A = 30$ cm/s without thermal radiation heat transfer. The white curves indicate the stoichiometric mixture fraction.

transfer term removed. The results are shown in Figure 19 and Figure 20 for $v_A = 30$ and 5 cm/s, respectively, for the distributions of the axial velocity, temperature, and soot volume fraction. The peak flame temperature is once again noticed to depend on the coflow air velocity, Figure 19(b) and Figure 20(b). It can be observed through a comparison between the results shown in Figure 19 for $v_A = 30$ cm/s at 0 g and those shown in Figures 8(c), 9(c), and 10(c) that there are relatively small increases in the axial velocity when thermal radiation is removed; however, there are significant increases in temperature and soot volume fraction. At $v_A = 30$ cm/s and 0 g, thermal radiation not only lowers the peak temperature, which occurs low in the flame, by about 94 K, but drastically reduces the temperature in the centreline region by about 530 K around $z = 6.5$ cm, Figures 19(b) and 8(c). Clearly, the double peaked centreline flame temperature distribution shown in Figure 8(c) becomes single peaked one when thermal radiation is removed. These features are further illustrated in Figure 21 where the distributions of temperature along the flame centreline with and without thermal radiation are compared. Moreover, both the flame height and the visible flame height become much shorter if there were no thermal radiation, which can be attributed to the drastic increase in the flame temperature in the centreline region. The increased difference between the flame height and the visible flame height, Figure 19(c), is again owing to the much higher temperatures around the flame tip, which results in much higher concentrations of OH. The much higher temperatures and OH concentrations then result in earlier complete soot oxidation.

When thermal radiation is not accounted for, the structure of the flame at 0 g and $v_A = 5$ cm/s, Figure 20, is qualitative similar to that at 0 g and $v_A = 30$ cm/s shown in

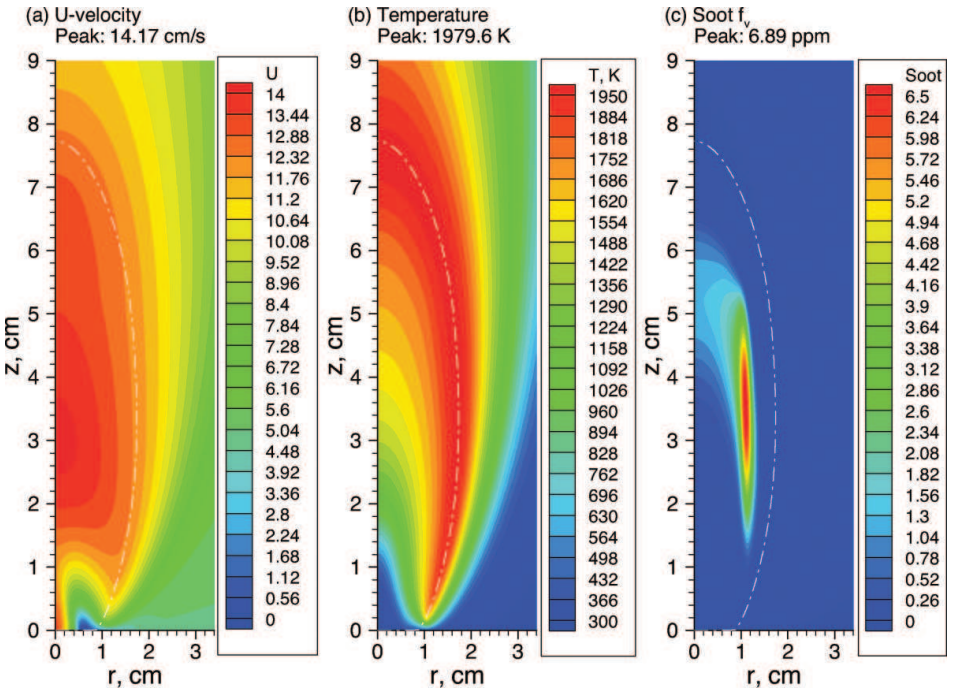

Figure 20. Distributions of axial velocity (in cm/s), temperature, and soot volume fraction (in ppm) at 0 g and $v_A = 5$ cm/s without thermal radiation heat transfer. The white curves indicate the stoichiometric mixture fraction.

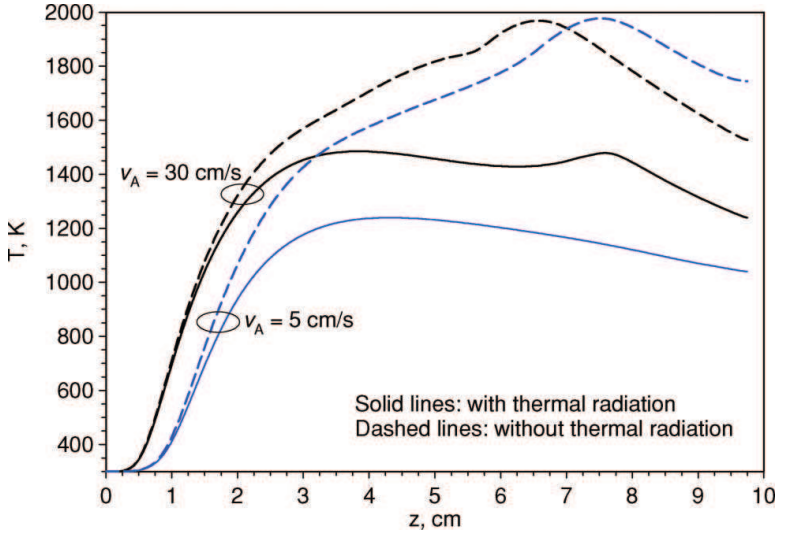

Figure 21. Effect of thermal radiation transfer on the temperature distributions along the flame centreline at 0 g for $v_A = 5$ and 30 cm/s.

Figure 19 and the above discussions hold. However, the effect of thermal radiation transfer now becomes much more pronounced with the peak temperature change by 192 K, and the centreline temperature changes by as much as 834 K at $z = 7.54$ cm, compare Figure 11(c) and Figure 20(b). The centreline temperature changes are clearly shown in Figure 21. Neglect of thermal radiation results in a completely different flame structure in terms of temperature and soot distributions. The soot concentrations increases by two orders of magnitude and the quenching in the centreline region does not occur anymore. The results summarised in Figures 19 to 21 clearly demonstrate that thermal radiation plays an extremely important role in determining the structure and soot formation behaviour of microgravity laminar diffusion flames.

4. Conclusion

The gravity effects on the flame structure and soot formation of a laminar coflow methane/air diffusion flame at atmospheric pressure under three coflow air velocities were systematically investigated using detailed numerical calculations. The important role of the coflow air velocity to the flame structure and soot formation at microgravity was demonstrated for the first time. The numerical results reproduce many of the flame phenomena observed in microgravity experiments conducted in quiescent air, namely in microgravity a laminar diffusion flame is in general wider and taller than its normal gravity counterpart. The elimination of buoyancy-induced flow acceleration in microgravity results in significantly lower streamwise and radial flow velocities, which enhance the relative importance of diffusion over convection, leading to a larger flame in both radial and streamwise directions. The absence of buoyancy induced flow acceleration at microgravity leads to much longer residence times, especially at low coflow air velocity. The prolonged residence times enhance two competing aspects of soot formation. On one hand, it benefits soot loading through longer available time for soot surface growth. On the other hand, longer residence times, along with larger flame size, enhance thermal radiation loss, which in turn lowers the flame temperature and therefore soot inception and growth rates. Under the present conditions, the enhancement of soot formation through prolonged residence times was observed when the coflow air velocity was decreased from 77.6 cm/s to 30 cm/s. When the coflow air velocity was further decreased from 30 cm/s to 5 cm/s, the suppression of soot formation by the prolonged residence time dominates its benefit to soot formation; therefore, the soot loading decreases.

The numerical results show that for the higher two coflow air velocity cases the peak soot volume fraction at 0 g is increased by a factor of about 2 to 3 compared with that at 1 g and for the lowest coflow air velocity case the peak soot volume fraction is actually drastically decreased with the flame being soot emitting and somewhat quenched to emit CO and unburned hydrocarbons. Under the conditions investigated in this study, the visible flame heights are in general shorter than that defined by the stoichiometric mixture fraction on the flame centreline.

At normal and half gravity, the flame is buoyancy controlled and the axial velocity is largely independent of the coflow air velocity. At microgravity, however, the flame is momentum controlled and the coflow air velocity strongly affects the axial velocity and therefore the residence times. The radial velocity distributions at microgravity display a distinguished feature from those at the half or the full gravity. Furthermore, the radial velocity distribution of the microgravity flame at $v_A = 5$ cm/s exhibits a region of radially outward motion in the centreline region just above the fuel jet, which does not exist for the two higher coflow air velocities.

The effect of the coflow air velocity was found to be relatively small at normal gravity. However, it becomes increasingly significant as the gravity level is reduced. At microgravity, the coflow air velocity has a huge influence on the flame structure, soot distribution, and even causes the flame to partially extinguish in the flame centreline region when it is sufficiently low. It was revealed through numerical calculations that thermal radiation heat transfer plays an extremely important role in microgravity diffusion flames, especially when the coflow air velocities are low, and is the mechanism responsible for the drastic temperature decreases in the upper portion of the centreline region.

Numerical results also show that the gravity level and the coflow air velocity alter the pathlines that soot follows relative to the flame sheet and the effect of thermophoresis is negligible in both normal and microgravity. Results of the present numerical study also imply that microgravity diffusion flame in quiescent air could potentially experience radiation-induced extinction when the fuel nozzle diameter is sufficiently large for a given fuel flow rate. This conjecture remains to be confirmed experimentally.

Acknowledgement

Financial support from NSFC under Grant No. 59886002, 59986004 and 50976115 is gratefully acknowledged.

References

[1] S.L. Olson and J.S. T'ien, *Buoyant low-stretch diffusion flames beneath cylindrical PMMA samples*, Combust. Flame 121 (2000), pp. 439–452.
[2] J.L.Torero, T. Vietoris, G. Legros and P. Joulain, *Estimation of a total mass transfer number from the stand-off distance of a spreading flame*, Combust. Sci. Technol. 174(11&12) (2002), pp. 187–203.
[3] T. H. Cochran and W. J. Masica, *An investigation of gravity effects on laminar gas-jet diffusion flames*, Proc. Combust. Inst. 13 (1971), pp. 821–829.
[4] R.B. Edelman, O.F. Forune, G. Weilerstein, T.H. Cochran and J.B. Haggard, Jr., *An analytical and experimental investigation of gravity effects upon laminar gas jet-diffusion flames*, Proc. Combust. Inst. 14 (1973), pp. 399–412.
[5] R.B. Edelman and M.Y. Bahadori, *Effects of buoyancy on gas-jet diffusion flames: experiment and theory*, Acta Astronautica 13 (1986), pp. 681–688.
[6] M.Y. Bahadori, R.B. Edelman, D.P. Stocker and S.L. Olson, *Ignition and behavior of laminar gas-jet diffusion flames in microgravity*, AIAA J. 28 (1990), pp. 236–244.
[7] M.Y. Bahadori, R.B. Edelman, R.G. Sotos and D.P. Stocker, *Radiation from gas-jet diffusion flames in microgravity environments*, AIAA paper 91–719, 29th Aerospace Science Meeting, Reno, NV, 1991.
[8] S. Mortazavi, P.B. Sunderland, J. Jurng, Ü.Ö. Köylü and G.M. Faeth, *Structure of soot-containing laminar jet diffusion flames*, AIAA paper 93-708, 31st Aerospace Sciences Meeting & Exhibit, Reno, NV, 1993.
[9] P.B. Sunderland, S. Mortazavi, G.M. Faeth and D.L. Urban, *Laminar smoke points of nonbuoyant jet diffusion flames*, Combust. Flame 96 (1994), pp. 97–103.
[10] C.M. Megaridis, D.W. Griffin and B. Konsur, *Soot-field structure in laminar soot-emitting microgravity nonpremixed flames*, Proc. Combust. Inst. 26 (1996), pp. 1291–1299.
[11] P.S. Greenberg and J.C. Ku, *Soot volume fraction maps for normal and reduced gravity laminar acetylene jet diffusion flames*, Combust. Flame 108 (1997), pp. 227–230.
[12] D.L. Urban, Z.-G. Yuan, P.B. Sunderland, K.-C. Lin, Z. Dai, K. Sun and G.M. Faeth, *Structure and soot properties of nonbuoyant ethylene/air laminar jet diffusion flames*, AIAA J. 36 (1998), pp. 1346–1360.
[13] F.J. Diez, C. Aalburg, P.B. Sunderland, D.L. Urban, Z.-G. Yuan and G.M. Faeth, *Soot properties of laminar jet diffusion flames in microgravity*, Combust. Flame 156 (2009), pp. 1514–1524.

[14] B. Konsur, C.M. Megaridis and D.W. Griffin, *Fuel preheat effects on soot-field structure in laminar gas jet diffusion flames burning in 0-g and 1-g*, Combust. Flame 116 (1999), pp. 334–347.
[15] B. Konsur, C.M. Megaridis and D.W. Griffin, *Soot aerosol properties in laminar soot-emitting microgravity nonpremixed flames*, Combust. Flame 118 (1999), pp. 509–520.
[16] D.L. Urban, Z.-G. Yuan, P.B. Sunderland, K.-C. Lin, Z. Dai and G.M. Faeth, *Smoke-point properties of non-buoyant round laminar jet diffusion flames*, Proc. Combust. Inst. 28 (2000), pp. 1965–1972.
[17] K.-C. Lin and G.M. Faeth, *Shapes of nonbuoyant round luminous laminar-jet diffusion flames in coflowing air*, AIAA J., 37 (1999), pp. 759–765.
[18] T. Vietoris, J.L. Ellzey, P. Joulain, S.N. Mehta and J.L. Torero, *Laminar diffusion flame in microgravity: The results of the minitexus 6 sounding rocket experiment*. Proc. Combust. Instit. 28 (2000), pp. 2883–2889.
[19] L. Brahmi, T. Vietoris, S. Rouvreau, P. Joulain, L. David and J.L. Torero, *Microgravity laminar diffusion flame in a perpendicular fuel and oxidizer stream configuration*, AIAA J., 43(2005), pp. 1725–1733.
[20] G. Legros, P. Joulain, J.-P. Vantelon, A. Fuentes, D. Bertheau and J.L. Torero, *Soot volume fraction measurements in a three-dimensional laminar diffusion flame established in microgravity*, Combust. Sci. and Tech., 178 (2006), pp. 813–835,
[21] A. Fuentes, S. Rouvreau, P. Joulain, J. -P. Vantelon, G. Legros, J.L. Torero and A.C. Fernandez-Pello, *Sooting behavior dynamics of a non-buoyant laminar diffusion flame*, Combust. Sci. and Tech., 179 (2007), pp. 3–19.
[22] M. Frenklach and H. Wang, *Detailed modeling of soot particle nucleation and growth*, Proc. Combust. Inst. 23 (1990), pp. 1559–1566.
[23] A.V. Krestinin, *Polyyne model of soot formation process*, Proc. Combust. Inst. 27 (1998), pp. 1557–1563.
[24] C.R. Kaplan, E.S. Oran and K. Kailasanath, *Gravational effects on sooting diffusion flames*, Proc. Combust. Inst. 26 (1996), pp. 1301–1309.
[25] C.R. Kaplan and K. Kailasanath, *Flow-field effects on soot formation in normal and inverse methane-air diffusion flames*, Combust. Flame 124 (2001), pp. 275–294.
[26] F.Liu, K.A. Thomson, H. Guo and G.J. Smallwood, *Numerical and experimental study of an axisymmetric coflow laminar methane–air diffusion flame at pressures between 5 and 40 atmospheres*, Combust. Flame 146 (2006), pp. 456–471.
[27] I.M. Kennedy, C. Yam, D.C. Rapp and R.J. Santoro, *Modeling and measurements of soot and species in a laminar diffusion flame*, Combust. Flame 107 (1996), pp. 368–382.
[28] M.D. Smooke, C.S. McEnally, L.D. Pfefferle, R.J. Hall and M.B. Colket, *Computational and experimental study of soot formation in a coflow, laminar diffusion flame*, Combust. Flame 117 (1999), pp. 117–139.
[29] F. Liu, H. Guo and G.J. Smallwood, *Effects of radiation model on the modeling of a laminar coflow methane/air diffusion flame*, Combust. Flame 138 (2004), pp. 136–154.
[30] M.D. Smooke, M.B. Long, B.C. Connelly, M.B. Colket and R.J. Hall, *Soot formation in laminar diffusion flames*, Combust. Flame 143 (2005), pp. 613–628.
[31] K.T. Walsh, J. Fielding, M.D. Smooke and M.B. Long, *Experimental and computational study of temperature, species, and soot in buoyant and non–buoyant coflow laminar diffusion flames*, Proc. Combust. Inst. 28 (2000) 1973–1979.
[32] F. Liu, H. Guo, G.J. Smallwood and Ö.L. Gülder, *Numerical modelling of soot formation and oxidation in laminar coflow non-smoking and smoking ethylene diffusion flames*, Combust. Theory Modelling 7 (2003), pp. 301–315.
[33] H. Guo, F. Liu, G.J. Smallwood and Ö.L. Gülder, *The flame preheating effect on numerical modelling of soot formation in a two-dimensional laminar ethylene-air diffusion flame*, Combust. Theory Modelling 6 (2002), pp. 173–187.
[34] R.J. Kee, J.F. Grcar, M.D. Smooke and J.A. Miller, *A Fortran program for modeling steady laminar one-dimensional premixed flames*, Report No., SAND85-8240, Sandia National Laboratories,1985
[35] K.M. Leung, R.P. Lindstedt and W.P. Jones, 1991, *A simplified reaction mechanism for soot formation in nonpremixed flames*, Combust. Flame 87 (1991), pp. 289–305.
[36] F. Liu, H. Guo, G.J. Smallwood and Ö.L. Gülder, *Effects of gas and soot radiation on soot formation in a coflow laminar ethylene diffusion flame*, J. Quantitative Spectroscopy and Radiative Transfer 73 (2002), pp. 409–421.

[37] F. Liu and G.J. Smallwood, *An efficient approach for the implementation of the SNB based correlated-k method and its evaluation*, J. of Quantitative Spectroscopy and Radiative Transfer 84 (2004), pp. 465–475.
[38] A. Soufiani and J. Taine, *High temperature gas radiative property parameters of statistical narrow-band model for H_2O, CO_2 and CO, and correlated-K model for H_2O and CO_2*, Int. J. Heat Mass Transfer 40 (1997), pp. 987–991.
[39] G.P. Smith, *et al*., available at http://www.me.berkeley.edu/gri_mech/.
[40] R.W. Bilger, S.H. Stårner and R.J. Kee, *On reduced mechanisms for methane-air combustion in nonpremixed flames*, Combust. Flame 80 (1990), pp. 135–149.
[41] Ö.L. Gülder, D.R. Snelling and R.A. Sawchuk, *Influence of Hydrogen Addition to Fuel on Temperature Field and Soot Formation in Diffusion Flames*, Proc. Combust. Inst. 26 (1996), pp. 2351–2358.
[42] R.J. Santoro, T.T. Yeh, J.J. Horvath and H.G. Semerjian, *The transport and growth of soot particles in laminar diffusion flames*, Combust. Sci. Tech. 53 (1987), pp. 89–115.
[43] F.G. Roper, C. Smith and A.C. Cunningham, *The prediction of laminar jet diffusion flame sizes: Part II. Experimental verification*, Combust. Flame 29 (1977), pp. 227–234.
[44] F.G. Roper, *The prediction of laminar diffusion flames sizes: Part I. Theoretical model*, Combust. Flame 29 (1977), pp. 219–226.
[45] R.E. Mitchell, A.F. Sarofim and L.A. Clomburg, *Experimental and numerical investigation of confined laminar diffusion flames*, Combust. Flame 37 (1980), pp. 227–244.
[46] K. Maruta, M. Yoshida, H. Guo, Y. Ju and T. Niioka, *Extinction of low-stretched diffusion flame in microgravity*, Combust. Flame 112 (1998), pp. 181–187.